

# Faint members of the Chamaeleon I cloud\*

F. Comerón<sup>1</sup>, G.H. Rieke<sup>2</sup>, and R. Neuhäuser<sup>3</sup>

<sup>1</sup> European Southern Observatory, Karl-Schwarzschild-Strasse 2, D-85748 Garching bei München, Germany (e-mail: fcomeron@eso.org)

<sup>2</sup> Steward Observatory, University of Arizona, Tucson, AZ 85721, USA (e-mail: grieke@as.arizona.edu)

<sup>3</sup> MPI Extraterrestrische Physik, Giessenbachstrasse 1, D-85740 Garching bei München, Germany (e-mail: rne@mpe.mpg.de)

Received 23 July 1998 / Accepted 23 November 1998

**Abstract.** We present a survey of the central  $\sim 100$  arcmin<sup>2</sup> of the Chamaeleon I star forming cloud, including objective prism spectroscopy in the H $\alpha$  region and deep imaging in the near-infrared. We estimate the expected number of very low mass objects within the survey, taking as a reference the higher mass members identified in previous studies, and assuming different ages and slopes of the initial mass function of the Chamaeleon I population. A new approach is introduced to estimate the contribution of background objects to the counts of low luminosity sources. This method takes advantage of the fact that the contribution of Chamaeleon I members should be negligible at the faintest magnitudes covered by our survey for any reasonable shape of the initial mass function.

$K$ -band source counts indicate the absence of a significant population of very low mass stars, implying that the initial mass function at very low masses, approximated by a power law, has a form  $\Phi(\mathcal{M})d\mathcal{M} \propto \mathcal{M}^{-1}d\mathcal{M}$  or flatter. This conclusion is in qualitative agreement with the discovery of six new emission line objects in the objective prism survey, and with the fact that only 2–3 faint objects are detected in the region of the  $(J - H)$ ,  $(H - K)$  diagram diagnostic of near infrared excesses of circumstellar origin. The masses of the new emission line objects, derived from recent pre-main sequence evolutionary tracks, are found to be near, and possibly below, the hydrogen burning limit, and their ages to be younger than  $3 \times 10^6$  years. One of them is found to be a bona-fide brown dwarf, and its detection in a deep ROSAT exposure makes it the first, and so far the only, brown dwarf known to emit X-rays (Neuhäuser & Comerón 1998, *Science*, 282, 83). The near-infrared properties of the H $\alpha$  emission objects suggest that, unlike at higher masses, strong H $\alpha$  emission near the hydrogen-burning limit is not accompanied by infrared excess detectable in the  $K$  band. Comparing the numbers of very low mass objects expected from  $K$  band counts with the number of new H $\alpha$ -emitting members, for which we derive individual masses and ages, we find that the spectroscopic survey samples the initial mass function completely, or nearly completely, down to the hydrogen-burning limit.

**Key words:** stars: low-mass, brown dwarfs – stars: luminosity function, mass function – stars: pre-main sequence – infrared: stars

## 1. Introduction

Does the process of star formation vary with the density of the natal cloud or with the rate at which its mass is being converted into stars? The molecular clouds in Chamaeleon, one of the most nearby star forming regions, contain a sparse population of young stellar objects and other signposts of recent star formation (Schwartz 1991). These clouds are therefore a prime site to probe star formation at the low-density, low-rate extreme.

A considerable observational effort has been devoted to follow up photometry and spectroscopy of Chamaeleon objects detected in H $\alpha$  (Gauvin & Strom 1992, hereafter GS92; Hartigan 1993) and X-ray surveys (Feigelson et al. 1993, Huenemoerder et al. 1994, Alcalá et al. 1995, 1997, Covino et al. 1997). Embedded sources, including possible protostars, have also been detected in molecular-line surveys (Reipurth et al. 1996) and in mid-infrared surveys carried out by IRAS (Baud et al. 1984) and ISO (Nordh et al. 1996). The near-infrared properties of young stellar objects have been used to identify possible new members in large scale surveys like DENIS (Cambrésy et al. 1998). These studies have probed the star formation history of the region, the coevality of weak-lined and classical T Tauri stars, and the correlation of the X-ray activity with bulk properties of the emitting stars. As a result, the properties of the stellar population of the Chamaeleon clouds are well known down to masses of a few tenths of a solar mass.

The very low mass stellar population, however, has remained largely elusive. The low surface density of young stellar objects inferred from observations of the more massive population implies that broad band surveys in the visible or the near infrared will detect mostly background, unrelated sources (Hyland et al. 1982). On the other hand, X-ray surveys published so far, even with ROSAT pointed observations, were limited to stars with bolometric luminosities higher than  $\sim 0.15 L_{\odot}$ , corresponding to masses higher than  $\sim 0.3 M_{\odot}$  for pre-main sequence objects with an age of  $3 \times 10^6$  years (D’Antona & Mazzitelli 1997).

---

Send offprint requests to: F. Comerón

\* Based on observations collected at the European Southern Observatory, Chile, program 58.E-0429.

The situation has been similar with available  $H\alpha$  surveys, where severe incompleteness appeared at masses below  $\sim 0.6 M_{\odot}$  (GS92). In both observational approaches, substantially longer exposure times with the available instrumentation are mandatory to probe the stellar initial mass function at masses near the stellar/substellar borderline.

To constrain the characteristics of the low mass stellar population of the Chamaeleon I cloud, we have carried out deep surveys of a  $100 \text{ arcmin}^2$  area in its most obscured region (Cambrésy et al. 1997), using *JHK* imaging and spectroscopy in the  $H\alpha$  region. This area has the highest concentration of identified pre-main sequence objects in the entire Chamaeleon complex, and thus the ratio of member to background objects can be expected *a priori* to be highest. We introduce a new method for deriving the population of very low mass Chamaeleon I members, even if the membership of individual objects cannot be established. A comparison to the observed *K*-band magnitude distribution allows us to constrain the slope of the initial mass function to be similar to the behavior in other regions with a higher density of young stellar objects – i.e., to be roughly flat if expressed in differential logarithmic mass units. In addition, we identify new faint young stellar objects by means of the excess near infrared emission associated with the presence of circumstellar material or by their  $H\alpha$  emission, and individual masses and ages are derived in the latter case. Masses for the new members are found to be near, and in some cases below, the hydrogen-burning limit. ROSAT archive observations with exposure times much longer than those of published X-ray surveys of this area are used to determine or to put stringent limits on the X-ray luminosities of the new members. One of them, a  $0.03\text{--}0.04 M_{\odot}$  brown dwarf, is clearly detected in X-rays (Neuhäuser & Comerón 1998, hereafter NC98).

Our observations and data reduction are described in Sect. 2. The results are presented in Sect. 3, and their interpretation is discussed in Sect. 4. We summarize our conclusions in Sect. 5.

## 2. Observations

### 2.1. *JHK* imaging

The near-infrared observations were obtained on 27, 28, and 29 March 1997, using the  $256 \times 256 \text{ pixel}^2$  NICMOS3-based IRAC-2b infrared camera at the ESO-MPI 2.2 m telescope in La Silla, Chile. Two additional half-nights were kindly made available to us on 4 and 5 April 1997.

We obtained a mosaic of 25 fields centered at the coordinates  $\alpha = 11^{\text{h}}07^{\text{m}}26^{\text{s}}$ ,  $\delta = -77^{\circ}36'50''$  (J2000.0), approximately coincident with the center of the darkest nebulosity in visible images of Chamaeleon I, as well as with the highest surface density of X-ray detected sources (Feigelson et al. 1993). The star CD -76° 486 is near the center of our mosaic. The frames cover an area of  $\Delta\alpha \times \Delta\delta = 10' \times 10'5$ . In general, adjacent fields had an overlapping strip about 10 pixels wide in common. However, due to a pointing problem of the telescope near the South celestial pole, a few narrow gaps exist along the North-South direction, amounting to  $\sim 12\%$  of the surveyed area.

Each field consisted of nine frames per filter, taken with  $5''$  offsets over a  $10'' \times 10''$  grid. Each frame was in turn the coadd of 6 individual exposures of 10 sec, providing a total exposure of 9 min per frame in each filter. Image reduction was performed under IRAF, using standard tasks and dedicated scripts. Due to the absence of nebulosity at infrared wavelengths, frames obtained in a single night of observation were median-filtered to construct flat fields in each filter. Median averaging of the frames of each field also yielded the sky frame to subtract from the object frame prior to shifting and adding. Bad pixels were rejected in this final step.

Objects were automatically found in each frame using the DAOFIND task under the NOAO's APPHOT package layered on IRAF. The fitting parameters were adjusted interactively, until the results of the object search were found to be satisfactory by comparison to a visual inspection of the frames. Next, digital photometry was performed on the detected objects using the PHOT task, also under APPHOT. The photometry was calibrated by observing the standard stars HD 84090 and HD 106807 (Carter & Meadows 1995). For the Chamaeleon fields, an aperture of  $5''$  was chosen in view of the point spread function and the crowding of the region. The magnitudes obtained were in general nearly independent of reasonable changes in the aperture, except for the faintest stars. Differences above the 0.02 mag level, which we take as an appropriate threshold on the internal accuracy, only began to appear for magnitudes above  $K = 16.5$ ,  $H = 17.0$ ,  $J = 18.0$ . We are confident that the sample is complete to those limits, as objects fainter by more than 0.5 mag were still detected by the automated finding procedure. However, these objects have been excluded from our study due to their poorer photometric accuracy.

Saturation was obvious for the brightest stars in the field. Comparing the magnitudes obtained by us to those published by Lawson et al. 1996 (hereafter LFH96) shows nonlinearity to be severe for stars with magnitude brighter than  $\sim 10.5$  in each filter. Consequently, we used our data only for  $m_K > 10.5$ , where the photometry generally agrees between the two surveys to  $\sim 5\%$ . Photometric accuracy to the 0.05 mag level is also suggested by intercomparing the observations of the standard stars observed each night.

In total, we obtained valid photometry for 206 objects<sup>1</sup>. Fig. 1 shows the  $(J - H)$ ,  $(H - K)$  diagram for the objects detected in all three bands, to which we have added the brighter members identified in earlier works. The solid lines indicate the locus occupied by dwarfs and giants according to the spectral type vs. color calibration of Bessell & Brett 1988. We have extended the dwarf branch toward later spectral types, whose colors are taken from Kirkpatrick et al. 1993. Starting at the position of the latest type considered by them, M9, we have plotted the reddening vector corresponding to the extinction law of Rieke & Lebofsky 1985. Departures from the normal extinction law in the near infrared have been noticed in some star forming regions such as R CrA (Wilking et al. 1997). However, in

<sup>1</sup> The list of positions and *JHK* photometry can be obtained from the authors upon request.

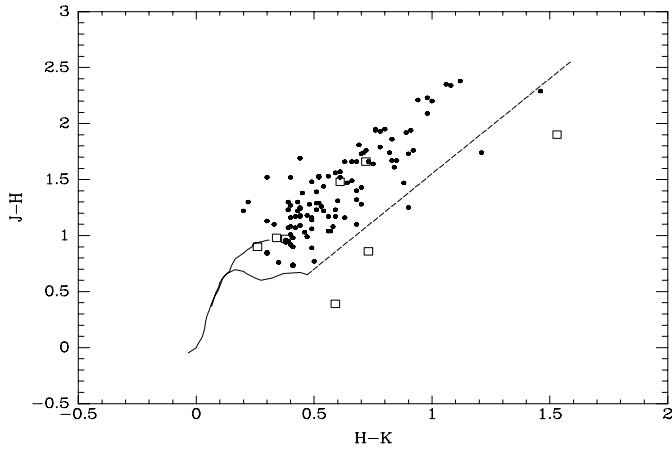


**Fig. 1.** Infrared color-color diagram displaying the position of the objects detected in our survey and with reliable magnitudes. The open squares correspond to 8 bright confirmed members in the surveyed area; the excluded object is HM 16, for which no published  $JHK$  photometry is available, and which was saturated in our images. We have used the  $JHK$  photometry provided by Lawson et al. 1996 for 7 of the objects; for CHXR 76 (= B34; Baud et al. 1984), whose  $H$  and  $K$  photometry is quoted as uncertain by Lawson et al., we have used instead our measured magnitudes,  $H = 11.32$ ,  $K = 10.94$ . The solid curves represent the locus of unreddened main sequence dwarfs (lower curve) and giants, and the dashed line is the normal reddening vector with  $E(J - H)/E(H - K) = 1.7$ . Its upper extreme corresponds to an extinction of  $A_V = 20$  mag.

the present case, the upper envelope of the distribution of stars in the  $(J - H)$ ,  $(H - K)$  diagram is parallel to the reddening vector, thus supporting our choice of extinction law.

Astrometry was performed using as a reference the positions of Chamaeleon I members listed in Appendix B of LFH96 (excluding HD 97048, for which their quoted position seems to be erroneous, probably due to the associated nebulosity as pointed out by Feigelson et al. 1993; the *Hipparcos* position was used instead). Because most frames do not contain stars appearing in that list, most positions were derived by using stars in the overlapping frame areas to refer to frames with position references. The overall astrometric precision is estimated to be better than  $5''$ .

## 2.2. Spectroscopy

The objective prism observations were carried out in the nights of 7 and 8 March 1998 using the Danish Faint Object Spectrograph and Camera (DFOSC) at the 1.5 m Danish telescope at the European Southern Observatory. We used a grism providing a dispersion of 22 nm/mm on the  $2k \times 2k$  pixels<sup>2</sup>,  $30.7 \text{ mm} \times 30.7 \text{ mm}$  detector. The spectral resolution is seeing-dependent, as no slit was used, and is estimated to be  $\lambda/\Delta\lambda \simeq 500$  from the resulting spectra. To eliminate contamination by background light, we used a Gunn  $r$  filter which isolated wavelengths between approximately  $6050 \text{ \AA}$  and  $7200 \text{ \AA}$ . The combined efficiency curve of the system (filter transmission, grating efficiency, and detector quantum efficiency) varies smoothly over

the useful spectral range, as was confirmed by inspection of the spectra of the earliest-type stars in our images. In addition, two images were obtained in the V and I filters to enable reliable source identification in the spectroscopic frames and to perform approximate digital aperture photometry in the visible. The center of the field is the same as for the  $JHK$  observations described above.

Eight individual objective prism images, each of 1800 seconds of exposure time, were obtained with small offsets of the telescope in between. The sky background in these frames was high enough to permit the construction of a flat field by stacking all the images together without correcting for the offsets. This was done by first normalizing the counts in each bias-subtracted frame to the background level of an empty control region, to correct for the varying background illumination level. The values obtained at each pixel position in the normalized frames were then median-averaged, rejecting the values deviating significantly from the average. Each individual, bias-subtracted image was then divided by the normalized flat field. The flat-fielded images were finally coadded, each one shifted as determined from the centroids of the  $H\alpha$  emission of selected stars.

The combined objective prism image was inspected for traces of  $H\alpha$  emission. The spectra selected in this way were extracted using the NOAO APEXTRACT package layered on IRAF. The individual spectra were wavelength calibrated in an approximate way, using as reference wavelengths the peak of  $H\alpha$  emission and, for the latest stars, the peak of the rather sharp feature lying between broad TiO absorption bands at  $7045 \text{ \AA}$ . For stars earlier than M0, the TiO bandhead at  $6875 \text{ \AA}$  provided a more accurate reference and was used instead. The positions of the newly detected  $H\alpha$  sources, labeled 1 to 6, are indicated in Fig. 2 on our I-band image of the area, along with other known Chamaeleon I members. Spectra are presented in this paper for all of these sources with the exception of the two brightest ones, HD 97048 and LkH $\alpha$  332-17, whose spectra appear saturated; and of CHXR26, whose spectrum is strongly contaminated by that of B 34. Given the larger field of view of DFOSC compared to the infrared survey, spectra were obtained for some Chamaeleon I members not observed in the infrared.

Digital photometry was performed on the V and I images in the same way as for the  $JHK$  observations. Apertures 9 pixels ( $=4''3$ ) in diameter were used, although the results were found to be generally insensitive to the aperture size. The magnitude zeropoint was calibrated by taking the values published by GS92 and LFH96 for some of the brighter stars in the field. The zeropoints derived from each individual star were found to be consistent to within 0.05 magnitudes. An exception was the star CHXR 78 NE, for which LFH96 give  $V = 12.88$ , indicating it was 1.2 magnitudes brighter than in our data: the quoted value makes it of similar brightness to Glass I, another star in the field, while it is clearly much fainter in our image. To our knowledge, however, the star has not been classified as variable, and has been considered as unrelated to the cloud by Huenemoerder et al. 1994.

A comparison with deep X-ray pointed observations from the ROSAT data archive revealed that the source labelled as

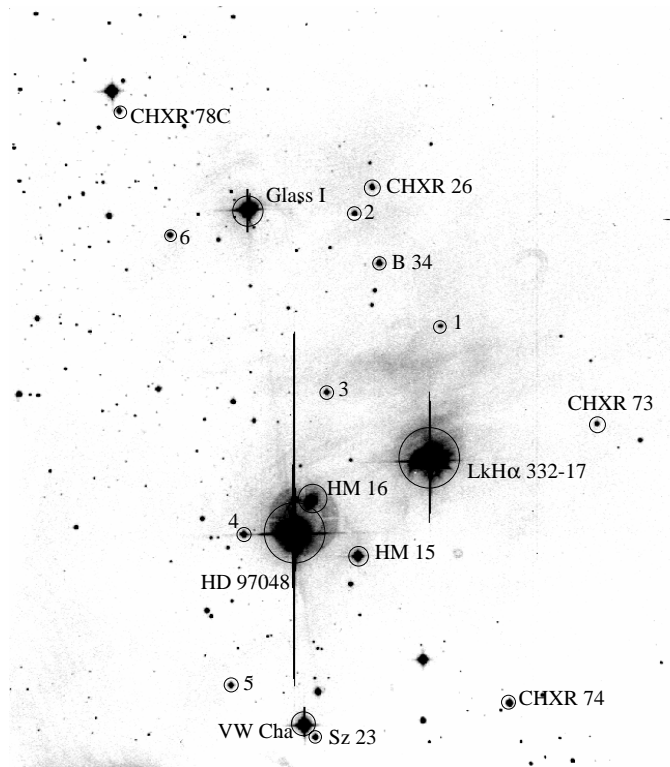


**Fig. 2.** Finding chart for the emission line objects discussed in this paper. The newly detected members are labeled from 1 to 6, while the principal denomination of LFH96 has been used for previously known members.

1 (hereafter Cha H $\alpha$  1) in Fig. 2 was the only clear X-ray detection among the newly identified emission line objects (see Sect. 3.5, and also NC98). This is a very faint object producing a barely visible continuum in the objective prism image, from which no reliable determination of the spectral type could be made. At the same time, its very low luminosity indicated a mass probably well below that of the other H $\alpha$  emitting objects, and possibly substellar. All this made it very desirable to obtain follow-up observations of this source, aimed at obtaining better quality spectra from which its position in the H-R diagram and its physical parameters could be reliably ascertained. Spectra in the visible and the near infrared of Cha H $\alpha$  1 were obtained with the ESO New Technology Telescope (NTT) on La Silla in May 1998; see NC98 for technical details on these observations.

### 2.3. X-ray observations

Apart from the flux-limited ROSAT All-Sky Survey observation (cf. Alcalá et al. 1995), the Chamaeleon I dark cloud members have been observed twice with the Positional Sensitive Proportional Counter (PSPC) (Pfeffermann et al. 1988) onboard ROSAT (Trümper 1983). We have retrieved from the ROSAT data archive a 32 ksec ROSAT pointed observation (# 200207) obtained on 1 February 1991 for H. Zinnecker as Principal Investigator (PI). We merged these data with a 5 ksec PSPC pointed observation (# 200046), also centered on Chamaeleon I, which

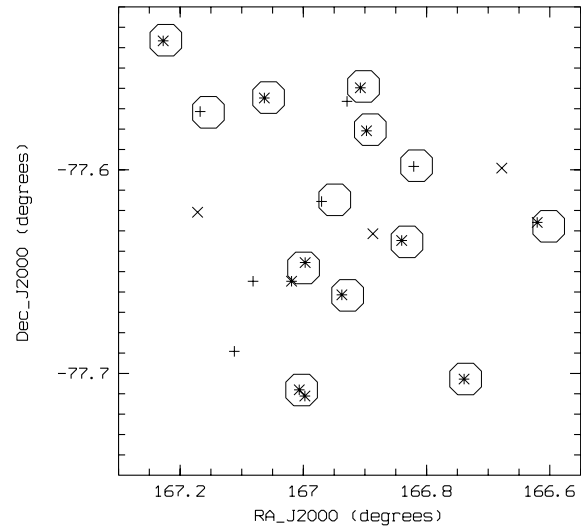


**Fig. 3.** Summary of the correspondences between objects detected in the infrared, H $\alpha$ , and X-ray surveys. Indicated are previously known members of Chamaeleon I (\*), the new emission line objects (+) and the new sources with near-infrared excess (X). The polygons indicate the ROSAT PSPC positions of sources detected with a confidence level above  $3\sigma$ .

was obtained in March 1991. These additional data are not yet in the ROSAT archive, but we can use them by courtesy of Prof. Eric Feigelson, the PI. The ROSAT All-Sky Survey exposure times are much smaller (below 1 ksec), so that we do not consider them here, but see Alcalá et al. 1995.

We performed standard local and map source detection algorithms with EXSAS version April 1998 (Zimmermann et al. 1994) running under ESO-MIDAS version Nov 1997 to reduce the merged data set and found that  $\sim 2''$  ( $20''$ ) can be allowed for the identification of bright (faint) X-ray sources with optical counterparts (see Fig. 3). The probability  $P$  for existence of a source is estimated as maximum likelihood  $ML$  with  $ML = -\ln(1 - P)$ . A value of, e.g.,  $ML = 14.3$  (or 5.9) corresponds to a detection significance of 5 (or 3) Gaussian  $\sigma$ . Some results from the short 5 ksec pointing were already published in Feigelson et al. 1993, but since we are dealing mainly with very late-type stars, which are very faint both in the optical and X-ray wavelengths, most of them were not detected in the short pointing, but only in the merged data set. A preliminary analysis of the long 31 ksec pointing was performed by Braun 1992, whose source list and X-ray data are in good agreement with our data (Sect. 3.5). The merged ROSAT PSPC image of the Chamaeleon I dark cloud is shown in NC98.

## 3. Results

A problem in studying the very low mass population of Chamaeleon I is separating the cluster members from the unrelated background objects, which dominate the overall source counts. In principle, this may be done if one can identify cluster members by some of the unique signatures displayed by young stellar objects, such as X-ray or H $\alpha$  emission, near-infrared ex-

cess, or variability. However, some objects may not display these phenomena; moreover, these signatures are a poorly known function of the mass or the age of the young stellar object. It is therefore desirable to estimate the number of members of the young stellar aggregate using a procedure that is as independent as possible of their individual identification through these signatures.

### 3.1. A new method for background subtraction

In relatively rich clusters, such an estimate can be achieved by comparing on-cluster and off-cluster star counts, applying a reddening model to the off-cluster counts, and subtracting them from the on-cluster values (e.g., Luhman and Rieke 1998; Luhman et al. 1998). However, in a very poor aggregate such as Chamaeleon I, we were concerned about possible subtle differences between an off field and the true cluster background that might introduce biases in the subtraction. In addition, unless a huge off-cluster area is surveyed, the background correction at the lowest cluster masses has a statistical weight similar to the cluster counts, and the subtraction yields a low significance for the counts of low mass objects. Therefore, we have developed a new method in which deep imaging data purely on the cluster can be used to calibrate and remove the background counts at high statistical weight.

Our approach is based on the substantial difference in slope between the  $K$  luminosity function in a young cluster and the  $K$  counts on the background. For example, from the D’Antona & Mazzitelli 1997 tracks, the mass-luminosity relation between 0.1 and  $1 M_{\odot}$  at  $3 \times 10^6$  years is  $L \sim \mathcal{M}^{1.5}$ , and the mass -  $K$  luminosity function is flatter still,  $L_K \sim \mathcal{M}^{1.2}$ . It has been found in a number of clusters that the low mass IMF is roughly flat in logarithmic units. Then, because the exponent in the mass- $L_K$  relation is close to 1, the predicted  $K$  luminosity function (in magnitudes) is virtually flat. In contrast, using the simplest geometric approximation, the counts in an infinite, extinction-free three dimensional stellar population should go as  $10^{\beta m}$ , where  $m$  is the magnitude and  $\beta = 0.6$ .

So long as they can be approximated by such exponentials, the form of these distribution functions is preserved for a young population embedded at varying depths in a clumpy cloud, as well as for a background population seen through a screen of variable extinction. This is straightforward to show for the background population. Let us assume that  $k 10^{\beta m} dm$  is the unobscured apparent magnitude distribution of the background: if we call  $q(A) dA$  the fraction of the surveyed area having a foreground extinction between  $A$  and  $A + dA$ , the “obscured” distribution function becomes

$$N(m) dm = \left( \int_{A=0}^{\infty} k q(A) 10^{\beta(m-A)} dA \right) dm \quad (1)$$

which can be written as

$$N(m) dm = k' 10^{\beta m} dm \quad (2)$$

with

$$k' = \int_{A=0}^{\infty} k q(A) 10^{-\beta A} dA, \quad \int_{A=0}^{\infty} q(A) dA = 1$$

Analogous expressions are found for the embedded population, if  $q(A) dA$  is now understood as the probability that the foreground extinction in front of a given source of the aggregate is comprised between  $A$  and  $A + dA$ . The complications arising from the structure of the obscuring clumpy molecular cloud are thus engulfed in  $k'$ , leaving  $\beta$  unaffected. As a result, the observed counts from any embedded cluster should include an approximately flat magnitude distribution from the cluster members, with a rapidly rising distribution of background counts at the faint end if the data are sufficiently deep to penetrate the obscuring cloud. Examples of this behavior can be found in Luhman and Rieke 1998 and Luhman et al. 1998.

The conventional on-cluster versus off-cluster subtraction is based on modeling  $k'$  and modifying the off-cluster counts accordingly to estimate the background. However, the slope invariance of the background counts lets us instead derive  $k'$  by normalizing to the faint end of the observed  $K$  magnitude distribution, if it is sufficiently below the inflection in the number counts. In addition, if the data are deep enough so the faint background counts are large, the subtraction can be made at high statistical weight even for brighter levels where the counts are small.

### 3.2. Application to Chamaeleon I

#### 3.2.1. Background population

Because the Galaxy is not infinite and due to other effects, the background stellar counts do not rise as steeply as  $\beta = 0.6$  from the simple geometric model. An accurate modeling of the galactic structure as traced by different classes of objects thus becomes necessary to accurately predict the expected stellar counts in any given direction. Wainscoat et al. 1992 have produced such a model to predict point source counts in the mid infrared, finding as a byproduct expected star counts at shorter wavelengths as well. A comparison with actual star counts, discussed by those authors, finds an excellent match between observations and model predictions, except at very small angular distances from the galactic equator where modeling uncertainties and extinction effects can produce significant departures. However, these effects are not expected to be important at the  $b = -16^\circ$  of our survey. The comparison between model predictions and K-band star counts in Wainscoat et al.’s work is not extended up to the  $K = 16.5$  limit of our survey, but the very good match that is achieved in their comparison with high latitude V-band data at much fainter magnitudes gives us confidence in that the model predictions should also be useable over the whole magnitude range of our survey. Wainscoat et al. find that the apparent magnitude  $m$  distribution in the  $K$ -band away from the galactic plane is very well represented by an exponential law of the form  $N(m)dm = k 10^{\beta m} dm$ , where  $k$  is a normalization factor, and  $\beta$  varies slowly with galactic latitude: at  $l = 90^\circ$ , it changes from 0.30 at  $b = 10^\circ$  to 0.32 at  $b = 30^\circ$ . We therefore adopt  $\beta = 0.31$  for the present case. Since theoretical models predict a rapid decrease of the  $K$  band luminosity with decreasing mass for very young objects with  $K \sim 14$  at

the distance of Chamaeleon I, and the survey is complete to  $K = 16.5$ , the counts at the faint end of the distribution will contain a negligible portion of cluster members.

We should point out that the adoption of the index  $\beta$  of the magnitude distribution of background sources as an external input parameter is not strictly necessary for our assessment on the contents of the aggregate, as long as a power law is indeed a good approximation. Model results are used in order to fix the value of  $\beta$  in Eq. (1), but the observations alone would already allow its independent determination, provided that the condition of a negligible contribution of aggregate members to the star counts at faint magnitudes is fulfilled. In this respect, the validity of the assumption of a power law, and of its adopted index, as an appropriate representation of the background distribution of magnitudes in our case can be assessed from the observed magnitude distribution. This will be discussed again in view of the results obtained at the end of Sect. 3.2.2.

### 3.2.2. Expected number of Chamaeleon I sources

To model the number of very low mass members of the Chamaeleon I aggregate, we assume that the region contains a population of coeval sources embedded at different depths in the molecular cloud, with a maximum foreground extinction  $A_{max}$ . The extinction towards a given source is assumed to have a random value between 0 and  $A_{max}$ , and the survey is assumed to be limited to, and complete in, the apparent magnitude interval  $m_1$  to  $m_2$  ( $m_1 > m_2$ ). If the initial mass function of the population is  $\Phi(\mathcal{M})$ , with  $C\Phi(\mathcal{M})d\mathcal{M}$  being the number of objects with masses between  $\mathcal{M}$  and  $\mathcal{M} + d\mathcal{M}$ , then the total number  $N$  of objects expected in the magnitude-limited sample is

$$N = \int_{A=0}^{A_{max}} dA \int_{M=m_1-DM-A}^{m_2-DM-A} C\Phi(\mathcal{M}(M)) \frac{d\mathcal{M}}{dM} dM \quad (3)$$

where  $M$  is the absolute magnitude at the reference wavelength of a star of mass  $\mathcal{M}$ , and  $DM$  is the distance modulus of the region.

We have applied Eq. (3) to our  $K$ -band results, with  $m_1 = 16.5$  and  $m_2 = 10.5$ , as discussed above. We have adopted  $DM = 6.0$  for Chamaeleon, corresponding to a distance of 160 pc (Whittet et al. 1997) which is supported by recent *Hipparcos*-based determinations (Wichmann et al. 1998, Knude & Høg 1998). The  $\mathcal{M}$  to  $M_K$  transformation for a given age has been derived from the theoretical pre-main sequence tracks of D’Antona & Mazzitelli 1997; we list in Table 1 the model masses, luminosities, and temperatures as a function of the age for unreddened objects at the  $K = 10.5$  bright limit of our survey. Our  $\mathcal{M}$  to  $M_K$  transformation ignores the possibility of infrared excesses of circumstellar origin, which could be noticeable in the  $K$  band. However, as will be discussed in some detail in Sect. 3.5, very few objects in our sample appear to display such excesses. Table 1 demonstrates that our survey probes from masses destined to settle near the bottom of the main sequence downward into the brown dwarf regime. Although the lower magnitude limit corresponds to masses of  $\sim 0.02 M_{\odot}$ , ob-

**Table 1.** Physical parameters at  $K = 10.5$

age (Myr)	$\mathcal{M}$ ( $M_{\odot}$ )	$L$ ( $L_{\odot}$ )	$T$ (K)
1	0.10	0.10	3000
3	0.25	0.12	3350
10	0.55	0.14	3750

**Table 2.** Known Chamaeleon I members in the surveyed area

Name	$\alpha$ (2000)	$\delta$ (2000)
CHXR 73	11:06:28.9	-77:37:33.0
CHXR 74	11:06:57.4	-77:42:10.4
LH $\alpha$ 332-17	11:07:20.8	-77:38:03.3
B 34	11:07:35.4	-77:34:50.7
CHXR 26	11:07:37.1	-77:33:32.9
HM 15	11:07:45.0	-77:39:40.6
HM 16	11:07:59.3	-77:38:43.9
HD 97048	11:08:04.6	-77:39:17
Glass I	11:08:15.2	-77:33:52.7

*Note:* All the coordinates are from LFH96, with the exception of HD 97048, for which they were taken from the SIMBAD database.

jects near this limit will contribute negligibly to the counts due to the small value of  $d\mathcal{M}/dM$  predicted by pre-main sequence tracks.

To evaluate Eq. (3), we need to determine two free parameters,  $A_{max}$  and  $C$ . The maximum extinction  $A_{max}$  is a rather ill-defined quantity, due to the clumpiness of molecular clouds. As most of the sources plotted in Fig. 1 are expected to be background, their scatter along the reddening line reflects the variable extinction along different lines of sight. For typical molecular clouds with a clump mass spectrum characterized by a power law of slope  $-1.6$ , Comerón et al. 1996b estimated that the scatter in extinctions along the line of sight is characterized by a dispersion  $\sigma \simeq 0.5A_{bg}$ , where  $A_{bg}$  is the average background extinction; i.e., the scatter is comparable to the extinction itself. In view of Fig. 1, we have used  $A_{K_{max}} = 1.2$  for our calculations, corresponding to  $A_V = 10.5$ . This is somewhat higher than the value of  $A_V = 7$  found by Cambrésy et al. 1997 from star counts, but the difference can be understood as due to the lower spatial resolution provided by the method employed by those authors in regions of higher extinction. Since very few cluster members are expected near the faint end of our sample, and since objects intrinsically brighter than  $K = 10.5$  but obscured above that threshold by the intervening extinction should not be very abundant, the value of  $A_{max}$  is not critical for our estimates.

The scaling factor  $C$  is estimated from the number of confirmed members in the area of our survey, assuming that they sample the mass function completely down to a mass  $\mathcal{M}_{min}$ . Table 2 lists these stars, for which LFH96 provide individual mass and age estimates based on two different sets of isochrones. We have obtained new derivations of these quantities using our spectroscopy and new sets of pre-main sequence evolutionary

**Table 3.** Expected numbers of faint Chamaeleon I members

age (Myr)	$\Phi(\mathcal{M}) \propto \mathcal{M}^{-\alpha}$		
	$\alpha = 1.5$	$\alpha = 1$	$\alpha = 0.5$
<i>a) predicted members sampling the IMF down to <math>0.4 M_{\odot}</math></i>			
1	79	29	13
3	86	38	25
10	54	36	32
<i>b) predicted members sampling the IMF down to <math>0.2 M_{\odot}</math></i>			
1	44	16	7
3	47	21	14

tracks by Burrows et al. 1993, 1997 and D’Antona & Mazzitelli 1997. Our new results are discussed in Sect. 3.4.

At least eight of these stars are detected X-ray sources. The ninth one, HM 16, is probably a weak X-ray emitter too, as can be seen in Fig. 3 of Feigelson et al. 1993, as well as in our Fig. 3 and in Fig. 1 of NC98: this elongated source is actually closer to HM 16 than to their proposed counterpart, HD 97048, which is more likely to be associated with another faint peak southeast of their source 29. Taking the new evolutionary tracks and the relation  $L_x/L_* = 1.6 \times 10^{-4}$  (Feigelson et al. 1993), the X-ray sample extends on average to  $\sim 0.2 M_{\odot}$ . However, the dispersion in the luminosity ratio implies that some sources will begin to be missed in the X-ray sample at  $0.4 M_{\odot}$ , and that some objects may be included at  $0.1 M_{\odot}$  if the X-ray to bolometric luminosity relation extends to this low mass range (see below). Therefore, for a flat IMF, we can assume an effective completeness limit of  $0.2 M_{\odot}$ . To show the dependence on this value, we have considered cases with  $\mathcal{M}_{min} = 0.4 M_{\odot}$  and  $\mathcal{M}_{min} = 0.2 M_{\odot}$ .

We have modeled the initial mass function  $\Phi(\mathcal{M})$  assuming it to have the shape given by Miller & Scalo 1979 down to a mass of  $0.2 M_{\odot}$ . The only role of the adopted mass function above this mass is the derivation of the normalization factor  $C$ , which is otherwise little sensitive to the shape of the mass function in that interval: for instance, assuming that its slope is constant and equal to  $-2.35$  (i.e. the classical Salpeter mass function) all the way down to  $0.2 M_{\odot}$  would change  $C$  by less than 30%. This is a rather extreme example, as no star forming region is known to have such a steep mass spectrum at low masses, and it can be used to illustrate the fact that the choice of  $\mathcal{M}_{min}$  and the uncertainties of the small number statistics are expected to have a far greater influence on our results. For masses below  $0.2 M_{\odot}$ , a power law is assumed, with varying exponents: the values considered,  $\Phi(\mathcal{M}) \propto \mathcal{M}^{-1.5}$ ,  $\propto \mathcal{M}^{-1}$ , and  $\propto \mathcal{M}^{-0.5}$ , cover practically all the range of initial mass functions observationally derived in numerous studies on the field and on clusters.

Table 3 lists the number of low mass Chamaeleon members expected to have  $10.5 < K < 16.5$ , for different assumptions concerning the age, the shape of the initial mass function, and the range of masses sampled by the confirmed members. The general trends appearing in Table 3 can be understood using qualitative arguments: if the known members are distributed

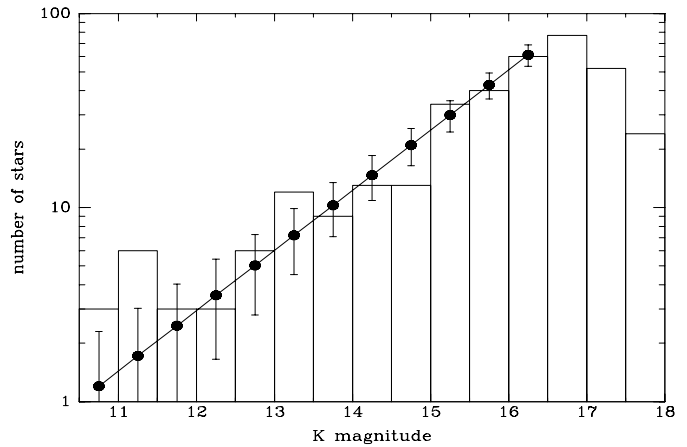


**Fig. 4.** Histogram of observed  $K$  magnitudes. The connected dots represent the values expected from a fit to the Wainscoat et al. 1992 background source distribution, normalized to the observed number of objects with  $15 < K < 16.5$ . The error bars are  $\sqrt{N}$  times the values predicted by the normalized background model. The faintest bins are included to illustrate the completeness level of the survey; however, the photometry becomes inaccurate above  $K \simeq 16.5$ , and sources start to be missed by the automated detection procedure around  $K \simeq 17$ .

over a wider mass range (i.e., to  $0.2 M_{\odot}$  rather than only to  $0.4 M_{\odot}$ ), then  $C$  is smaller and fewer members are predicted. Concerning the dependence on the power law index  $\alpha$ , a steeply rising initial mass function towards smaller masses is expected to result in many more faint objects observed than in the case of a flatter initial mass function, explaining the decreasing numbers as we move from left to right in Table 3. On the other hand, the trends seen as we move from younger to older ages of the population are also the result of the evolution in luminosity of low mass objects. As the population ages, bright stars enter the interval of magnitudes considered here as their  $K$  magnitude increases over 10.5, while initially faint stars leave the interval as they fade beyond  $K = 16.5$ . Whether the total number of stars in the interval increases or decreases with time depends on two factors: the slope of the initial mass function, and the rate of decrease of the luminosity. Thus, although in all the cases assumed here the faint objects outnumber the bright ones, the number of stars in the interval can actually grow with time due to the slower evolution in luminosity of the less massive stars, provided that the slope of the initial mass function is shallow enough. This is the case for the shallowest slope considered here,  $\Phi(\mathcal{M}) \propto \mathcal{M}^{-0.5}$ , while for an initial mass function  $\Phi(\mathcal{M}) \propto \mathcal{M}^{-1}$  both effects nearly cancel out over the age interval 1 - 10 Myr.

The histogram of  $K$  magnitudes is shown in Fig. 4. As explained in Sect. 2.1, we consider the source detection and the photometry to be reliable up to  $K = 16.5$ ; we will therefore focus our discussion on the  $10.5 < K < 16.5$  interval. Also shown in Fig. 4 is the expected magnitude distribution of background stars, normalized to the number of detected stars with  $15 < K < 16.5$ , where the contribution of Chamaeleon I members should be negligible. This normalization may be affected

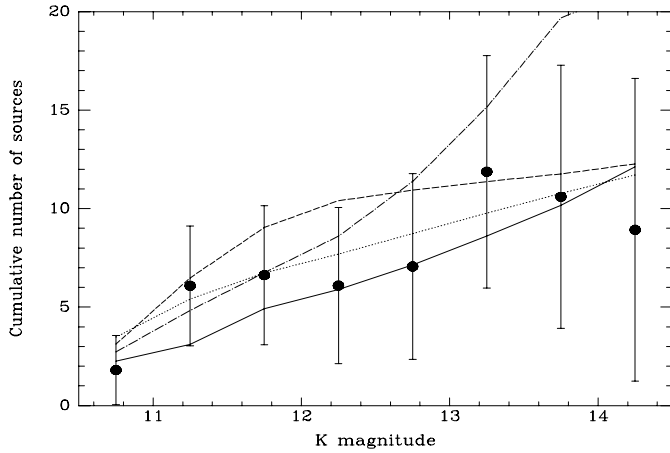


**Fig. 5.** Distribution of the excess of sources over the extrapolated background as a function of the limiting magnitude. The curves represent the distribution expected for some cases selected from Table 3: *a*) known members sampling the IMF down to  $0.2 M_{\odot}$ , age  $10^6$  yr,  $\alpha = 1$  (solid line); *b*) known members sampling the IMF down to  $0.4 M_{\odot}$ , age  $10^6$  yr,  $\alpha = 0.5$  (dotted line); *c*) known members sampling the IMF down to  $0.2 M_{\odot}$ , age  $3 \times 10^6$  yr,  $\alpha = 0.5$  (dashed line); *d*) known members sampling the IMF down to  $0.2 M_{\odot}$ , age  $10^6$  yr,  $\alpha = 1.5$  (dot-dashed line). The first three cases are those providing the best fit to the data. The last one is the best fitting case with  $\alpha = 1.5$ ; even so, it still predicts too many Chamaeleon members at moderately faint magnitudes.

by a bias due to the rising shape of the apparent magnitude distribution combined with the increasing photometric errors as one goes to fainter magnitudes: the larger number of objects for which we measure  $K > 16.5$  implies that more objects from the  $16.5 < K < 17.0$  bin will be erroneously assigned to the  $16.0 < K < 16.5$  bin than the opposite, thus leading to an overestimate of the objects with  $16.0 < K < 16.5$ . However, the internal consistency of the photometry (0.02 mag; see Sect. 2.1) at our adopted cutoff suggests that this bias should not be relevant in practice for the present case.

The observed distribution of  $K$  magnitudes shows a good overall agreement with the predictions of the background population model, with hints of an excess of observed objects at the brightest magnitudes that can be interpreted as the statistical signature of the Chamaeleon I population. Due to the small numbers of both predicted and observed objects, this excess is difficult to quantify. It is clear, however, that Fig. 4 argues against the existence of a large number of Chamaeleon I members in the interval  $10.5 < K < 16.5$ . For example, we can estimate the exponential index  $\beta$  of the background magnitude distribution that would be required if there were a minimum of 50 members with  $K < 15$  in the surveyed region, assuming that the counts are dominated by the background above  $K = 15$  (which should be the case, unless most of the sources that we detect are brown dwarfs with  $\mathcal{M} < 0.02 M_{\odot}$ !). We find that such a situation would require  $\beta > 0.6$ , this is, even steeper than in the extreme case of an infinite Galaxy without extinction.

A closer look at this excess is presented in Fig. 5. In it, we have calculated the excess of sources (i.e., the difference between the observed number of sources and

the extrapolated background) as a function of the limiting magnitude. The error bars reflect the  $\sqrt{N}$  uncertainties due to the limited-number statistics. Their length equals  $\sqrt{N_{\text{observed}} + N_{\text{background}}^2} / N_{\text{norm}}$ , where  $N_{\text{norm}}$  is the number of objects in the magnitude interval used to calculate the normalization factor of the background distribution function. The different curves represent selected examples of expected source counts as a function of limiting magnitude: they are derived from Eq. (3), using  $m_2 = 10.5$  and varying  $m_1$  to different limits. The examples plotted in Fig. 5 are the three providing the best fit to the data points, plus the best fit that can be obtained imposing an IMF slope  $\alpha = 1.5$ . Notice that the vertical scale is now linear, rather than logarithmic as in Fig. 4.

### 3.3. Objects with $H\alpha$ emission

In the core of IC 348, Luhman et al. 1998 show that 16 of 67 stars with spectral types of F or later have  $H\alpha$  equivalent widths of  $10 \text{ \AA}$  or greater. Over a larger region in this cluster, Herbig 1998 found 51 stars with  $H\alpha$  equivalent widths above this threshold out of a total of 109. These studies suggest that, in a low density region such as Chamaeleon I, about 40% of the very young stars might be expected to have detectable  $H\alpha$  in our survey. We assume that the embedded population is all sufficiently young that the  $H\alpha$  has not begun to fade ( $\leq 3$  million years). From Fig. 4, there are 6 embedded objects with  $10.5 < K < 11.5$ , corresponding to a total of  $\sim 7$  objects if we allow for the missing area in the infrared survey. We would predict that 40%, or 3, of these stars should have detectable  $H\alpha$ .

Figs. 6 and 7 show the spectra of 14 of the objects with detected  $H\alpha$  emission, identified in Fig. 2. The spectra plotted in Fig. 6 correspond to previously identified Chamaeleon I members; in six of the nine cases, spectral classifications were already available in the literature. Fig. 7 shows the spectra of five of our newly discovered faint members; Cha  $H\alpha 1$  is separately discussed at the end of Sect. 3.1.1. Table 4 summarizes the available photometry and the equivalent width measured for the  $H\alpha$  emission. Most photometric data come from the  $V$  and  $I$  images obtained as described in Sect. 2.2 and from the  $JHK$  survey described in Sect. 2.1. Exceptions are the brighter sources that appear saturated in those images or those lying outside the area of the  $JHK$  survey, for which values found in the literature are given instead when available. These cases are marked in Table 4. We note that photometry in other bands ( $U$ ,  $B$ ,  $R$ ,  $L'$ ) can be found as well for most of the brighter objects in GS92 and LFH96. Three of the new aggregate members can be found too in the USNO-PMM catalog, providing low precision  $B$  and  $R$  magnitudes which are quoted in the footnotes to Table 4. Where we predict three stars with detectable  $H\alpha$  in the interval  $10.5 < K < 11.5$ , we detect four, one with  $H\alpha$  equivalent width  $> 10 \text{ \AA}$ , one close to this value, and two near  $5 \text{ \AA}$ . This result agrees satisfactorily with our prediction and supports the assumption that the entire population is 3 million years or less in age.

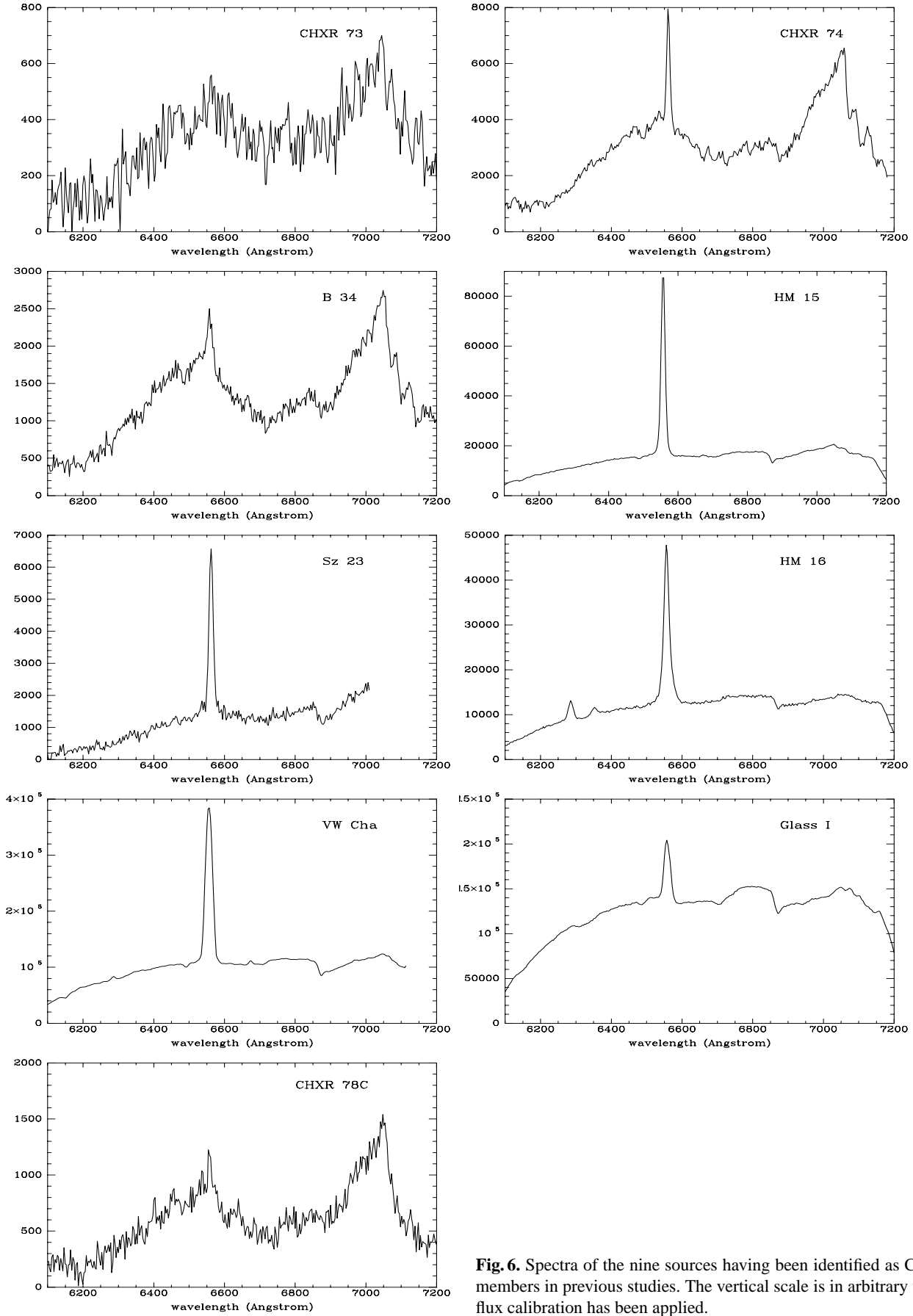


**Fig. 6.** Spectra of the nine sources having been identified as Chamaeleon I members in previous studies. The vertical scale is in arbitrary units, and no flux calibration has been applied.

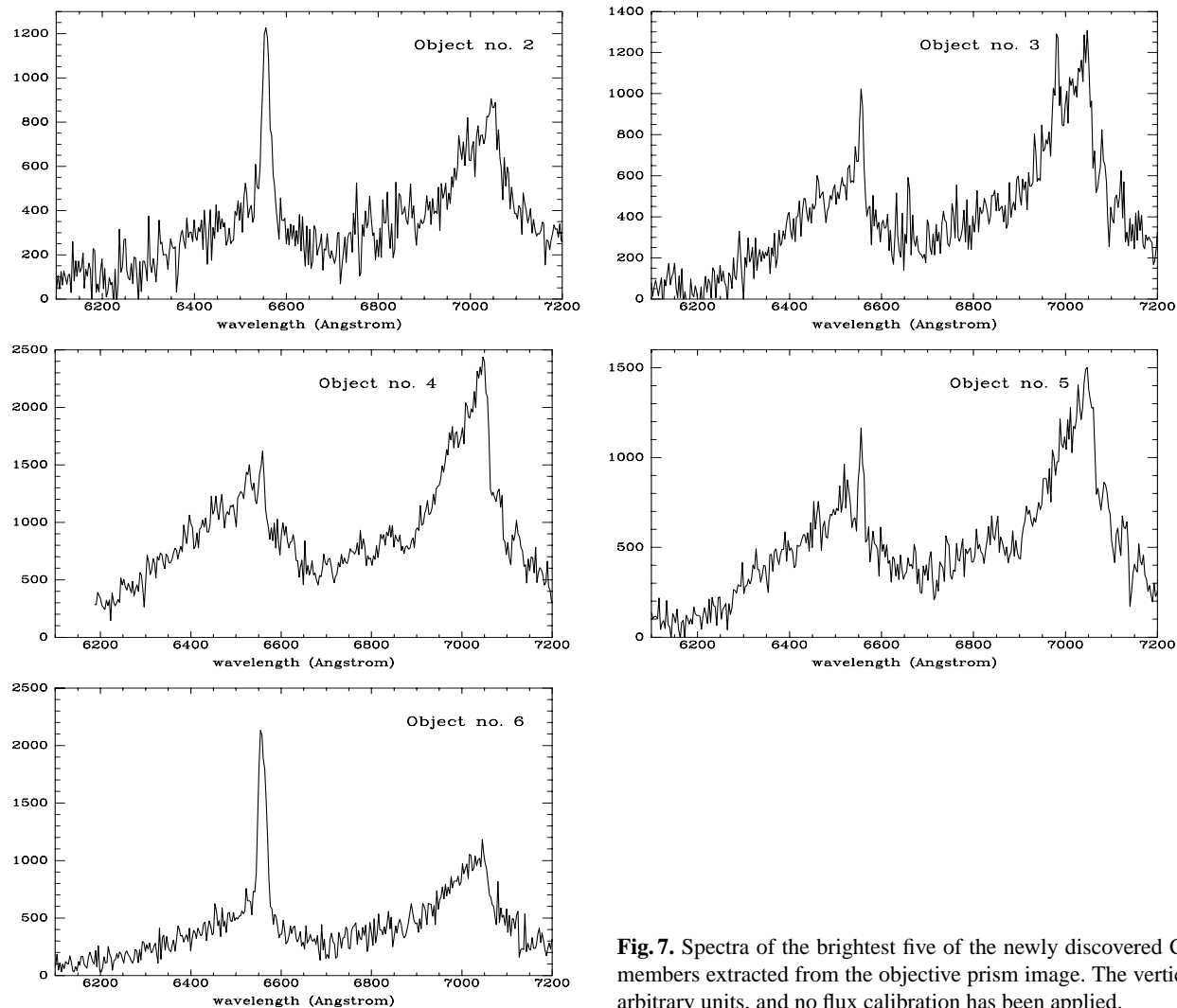


**Fig. 7.** Spectra of the brightest five of the newly discovered Chamaeleon I members extracted from the objective prism image. The vertical scale is in arbitrary units, and no flux calibration has been applied.

### 3.3.1. Spectral classification

Although the wavelength interval covered by our objective prism spectra spans only about 1000 Å centered around H $\alpha$ , it contains several features useful for spectral classification (e.g. Prosser et al. 1991, Williams et al. 1994, Martín et al. 1996). We will use the narrow synthetic bands  $R_2$ ,  $R_3$ ,  $R_4$ , and  $R_7$  of Prosser et al. 1991 for this purpose; their limits are listed in Table 5. The reader is referred to Prosser et al. 1991 for a detailed discussion of the correlation between flux ratios in these passbands and the spectral type. We note here that the fact that our spectra are not flux-calibrated does not have a noticeable impact on the derived ratios, as the system response does not change appreciably over the  $R_2 + R_3$  or the  $R_4 + R_7$  intervals, thanks to the fact that the passbands from which the ratios are calculated are narrow and adjacent. The ratios that we find are in general somewhat outside the limits of those considered by Prosser et al., thus indicating later spectral types than those considered in that work. However, given their proximity to the extreme values of the ratios found by those authors, and the fairly monotonic trends exhibited by the ratios between M0 and M5 (see Fig. 4

of Prosser et al.), we believe that the extrapolation to the ranges found here is a safe one. A possible exception is Cha H $\alpha$  1, that we classify using different criteria, as discussed below.

Table 6 lists the values of the  $R_4/R_7$  and the  $R_3/R_2$  ratios for all the stars whose spectra are presented in Figs. 6 and 7. To calculate the flux in the  $R_2$  band, we cut out the H $\alpha$  emission by interpolating the underlying pseudocontinuum between adjacent points. The spectral classification uses the weighting scheme proposed by Prosser et al. 1991, i.e., giving twice as much weight to  $R_4/R_7$  as to  $R_3/R_2$  for stars later than M0, and equal weight otherwise. This is not a critical choice, as we find that the spectral types defined by either index are usually within one spectral subclass of each other. Spectral types found in the literature for some of our objects are also given, and the overall agreement is found to be good. The only possible exceptions are CHXR 74, for which LFH96 find a rather uncertain, but apparently earlier spectral type than we do, and CHXR 73, a highly obscured object for which no good quality spectra have been obtained yet. The somewhat earlier spectral types given by GS92 to VW Cha and Glass I can be explained as due to the decrease in sensitivity to spectral type of the narrow band

**Table 4.** Photometry and H $\alpha$  equivalent width for all the objects observed

Name	$\alpha$ (2000)	$\delta$ (2000)	V	I	J	H	K	W(H $\alpha$ ) ( $\text{\AA}$ )	Notes
CHXR 73	11:06:28.9	-77:37:33	20.2	15.60	12.81	11.32	10.79	–	
CHXR 74	11:06:57.4	-77:42:10	17.27	13.59	11.55 <sup>b</sup>	10.57 <sup>b</sup>	10.23 <sup>b</sup>	13	
B 34	11:07:35.4	-77:34:51	18.09	14.31	12.29	11.32	10.94	5.5	
HM 15	11:07:45.0	-77:39:41	15.42	12.55 <sup>a</sup>	10.41 <sup>b</sup>	9.09 <sup>b</sup>	8.35 <sup>b</sup>	70	
Sz23	11:07:59.4	-77:42:40	18.04	14.40	–	–	–	45	out of the <i>JHK</i> survey
HM 16	11:07:59.3	-77:38:44	15.66:	–	–	–	–	61	<i>I, J, H, K</i> saturated
VW Cha	11:08:01.6	-77:42:29	13.16	10.61 <sup>a</sup>	8.91 <sup>b</sup>	7.75 <sup>b</sup>	7.08 <sup>b</sup>	64	
Glass I	11:08:15.2	-77:33:53	12.81 <sup>a</sup>	10.90 <sup>a</sup>	8.77 <sup>b</sup>	7.40 <sup>b</sup>	6.34 <sup>b</sup>	11	
CHXR78C	11:08:54.6	-77:32:12	18.98	14.76	12.41 <sup>b</sup>	11.64 <sup>b</sup>	11.28 <sup>b</sup>	3.2	
Cha H $\alpha$ 1	11:07:17.0	-77:35:54	21.0 <sup>c</sup>	16.23	13.55	12.78	12.28	59	
Cha H $\alpha$ 2	11:07:43.0	-77:33:59	20.4	15.11	12.59	11.43	11.15	39	
Cha H $\alpha$ 3	11:07:52.9	-77:36:56	19.42	14.90	12.46	11.64	11.11	4.5	
Cha H $\alpha$ 4	11:08:19.6	-77:39:17	18.67	14.35	12.20	11.42	11.04	4.7	
Cha H $\alpha$ 5	11:08:26.9	-77:41:21	19.68	14.69	12.14	11.21	10.76	7.6	
Cha H $\alpha$ 6	11:08:40.2	-77:34:17	19.75	14.97	–	–	–	59	out of the <i>JHK</i> survey

Notes on the photometry:

<sup>a</sup> photometry from GS92

<sup>b</sup> photometry from LFH96

<sup>c</sup> *V* measurement obtained with the ESO-NTT telescope on La Silla in July 1998; photometric accuracy is  $\pm 0.23$  mag.

Three of the new Chamaeleon I sources are found in the USNO-PMM catalog, from which rough *B* and *R* magnitudes ( $\pm 0.5$  mag) are derived. These are:

Cha H $\alpha$ 1: *B* = 23.3, *R* = 19.6.

Cha H $\alpha$ 2: *B* = 23.4, *R* = 18.9.

Cha H $\alpha$ 6: *B* = 23.1, *R* = 18.3.

**Table 5.** Narrow bands for M star classification (Prosser et al. 1991)

Band	limits ( $\text{\AA}$ )
<i>R</i> <sub>2</sub>	6507–6598
<i>R</i> <sub>3</sub>	6635–6718
<i>R</i> <sub>4</sub>	6750–6844
<i>R</i> <sub>7</sub>	7000–7068

indices for spectral types earlier than M0, which makes our classifications more uncertain.

The classification scheme based on the *R<sub>i</sub>* ratios described above is based on spectral types M5.5 and earlier, and may therefore be inappropriate to classify a clearly later-type object like Cha H $\alpha$  1, given the saturation that is often found for similar indexes at very low temperatures. Moreover, the much wider wavelength coverage available for this object thanks to the NTT spectra makes possible a much more robust classification based on other features. Here we discuss in some detail the derived spectral type for this object on the basis of different classification schemes that have been proposed for late M dwarfs, expanding the short discussion given in NC98.

A spectral sequence extending to spectral types as late as M9, documented with a large number of standards, has been proposed by Kirkpatrick et al. 1991, 1995. A comparison of composite spectra of stars classified in this scheme with Cha H $\alpha$  1 is shown in Fig. 8, which shows that the latter object must be clearly later than spectral type M6. This is especially well

**Table 6.** Spectral index ratios and classification

Name	<i>R</i> <sub>4</sub> / <i>R</i> <sub>7</sub>	<i>R</i> <sub>3</sub> / <i>R</i> <sub>2</sub>	Sp. type	notes
CHXR 73	0.59:	0.74:	M4.5:	K3-M2 in LFH96
CHXR 74	0.74	0.66	M4.5	K2-M2 in LFH96
B 34	0.72	0.61	M5	
HM 15	1.26	0.89	M1	M0.5 in GS92
Sz23	–	0.79	M2.5	R7 out of frame
HM 16	1.42	0.93	K7	
VW Cha	1.35	0.90	M0.5	K5 in GS92
Glass I	1.46	0.90	K7	K4 in GS92
CHXR78C	0.64	0.58	M5.5	M4-M6 in LFH96
Cha H $\alpha$ 1	–	–	M7.5-M8	from NTT spectra
Cha H $\alpha$ 2	0.59	0.50	M6	
Cha H $\alpha$ 3	0.55	0.53	M6	
Cha H $\alpha$ 4	0.55	0.48	M6.5	
Cha H $\alpha$ 5	0.54	0.53	M6	
Cha H $\alpha$ 6	0.57	0.50	M6	

seen by comparing the dependence on the temperature of the discontinuity in the slope of the spectrum near 8000  $\text{\AA}$ . The composite spectrum whose overall shape matches most closely the spectrum of Cha H $\alpha$  1 seems to be M8V.

Kirkpatrick et al. 1991 also provide a number of “color ratios” measuring the strength of different temperature-sensitive features that we can measure on the spectrum of Cha H $\alpha$  1. Ratio A, measuring the CaH feature at 6975  $\text{\AA}$ , peaks at spectral

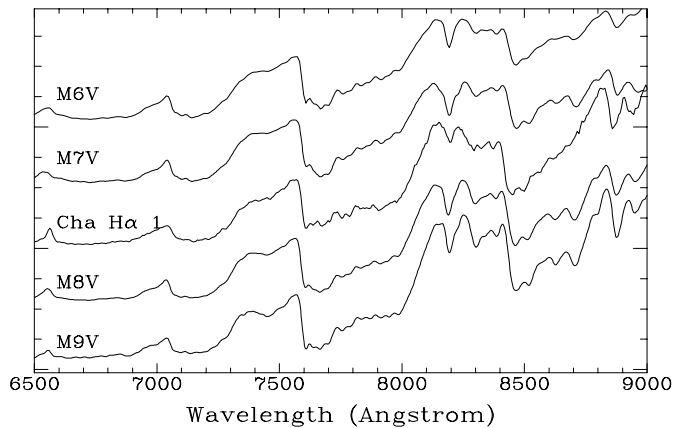


**Fig. 8.** A comparison of field M dwarf spectra (individual and composite) with the spectrum of Cha H $\alpha$  1. The M6V spectrum is that of Gl 406; M7V, that of vB 8; M8V is the combination of the spectra of LHS 2243, LHS 2397 A, LP 412-31, and vB 10; and M9V, that of BRI 1222-1222, LHS 2065, LHS 2924, and TVLM 868-110639. The spectral classifications are from Kirkpatrick et al. 1995. Note in particular the stronger NaI feature at 8190 Å in the field M dwarfs, indicating a lower surface gravity of Cha H $\alpha$  1.

type M6.5-M7, and the value measured for Cha H $\alpha$  1, 1.38, is found at spectral types M5 and M7.5-M8; the former possibility is ruled out by the overall appearance of the spectrum. Ratio B, measuring the TiI feature at 7358 Å, has a broad peak between M5.5 and M6; the value we measure, 1.11, is near the peak value. On the other hand, Ratio C, measuring the NaI features at 8183 and 8195 Å, is very low for our object at 1.05; such low values are found for spectral type standards M8 and later, but would be also expected as a surface gravity effect, as discussed below. Finally, Ratio D measuring the CaII feature at 8542 Å is also very low at 1.07. This index has a minimum near this value between M4 and M5, then rises at lower temperatures, and drops again to that level for stars later than M8. Therefore, with the possible exception of Ratio B, all the other color ratios consistently agree in classifying Cha H $\alpha$  1 as M7.5 or later.

Another set of color ratios, aimed at establishing a spectral sequence for young brown dwarfs, has been defined by Martín et al. 1996. These authors propose a quantification of the spectral subtype as a function of several pseudo-continuum spectral regions. Using their expressions for the spectral type as a function of the pseudo-continuum indexes PC3, PC4, and PC5, we find M spectral subtypes of 7.82, 8.28, and 7.01, respectively. The weighted average based on the standard deviation of the spectral subtype-pseudocontinuum index relationship yields a M7.8 type for Cha H $\alpha$  1. We note that the other two pseudocontinuum indexes, PC1 and PC2, both lie above the peak values found in the standard stars used by those authors, both in the proximities of M8. Finally, we have measured the VO ratio based on the absorption band produced by that molecule at 7445 Å, whose definition and advantages have been discussed by Kirkpatrick et al. 1995. The value obtained, 1.076, places Cha H $\alpha$  1 in subclass 8.

In summary, we find a remarkable overall agreement among all the classification criteria based on the red part of the visible spectrum, which almost unanimously assign a spectral type M7.5–M8 to Cha H $\alpha$  1. This classification is in good agreement with that derived from the spectrum in the 2  $\mu$ m region, discussed by NC98, which is dominated by a broad depression between the H and K bands due to water absorption in the photosphere of the star. Its depth cannot be accurately quantified due to strong telluric absorption in that region, but comparison with synthetic atmosphere models (Allard & Hauschildt 1995a) clearly suggests a temperature of 2800 K or lower.

The NaI feature around 8190 Å, known to decrease with decreasing surface gravity (Kirkpatrick et al. 1991), is clearly weaker in the spectrum of Cha H $\alpha$  1 than in those of any of the field M dwarfs shown for comparison. This is to be expected, as the surface gravity of a young stellar object should be intermediate between that of an evolved M dwarf (where NaI is strong) and that of a giant (where NaI is weak). A surface gravity effect in the same direction is also noticed in the NaI feature at 2.21  $\mu$ m, which is not visible in the spectrum of Cha H $\alpha$  1 (NC98), while it is a prominent feature in late field M dwarfs (Jones et al. 1994). Luhman & Rieke 1998, Luhman et al. 1998, and Wilking et al. 1998 also find a NaI feature systematically weaker than expected for a given spectral type, or even absent, in young stellar objects in L1495E and IC 348. The relative weakness of NaI absorption in the visible spectrum of Cha H $\alpha$  1, and its absence in the *K*-band spectrum, can thus be taken as a proof that it is a true young stellar object, and therefore a member of the Chamaeleon I aggregate, rather than an evolved foreground dMe star unrelated to the dark cloud population. The membership of Cha H $\alpha$  1 is independently supported by its noticeable infrared excess at longer wavelengths, which has been detected recently by ISOCAM on board of the Infrared Space Observatory at 6.75 and 15  $\mu$ m (Anlauf Amanda Kaas, private communication; Olofsson et al. 1998).

### 3.3.2. Luminosities and temperatures

The spectral classification and photometry presented in Tables 4 and 6 permit the placing of the Chamaeleon I objects in the H-R diagram, using temperature-spectral type calibrations plus intrinsic colors and bolometric corrections for late-type atmospheres. In turn, a comparison to the  $L$ - $T_{eff}$  loci predicted by theoretical pre-main sequence evolutionary tracks allows an estimate of the age and the mass of the objects.

We will use the compilation of intrinsic colors and bolometric corrections for main sequence stars by Kenyon & Hartmann 1995 to derive foreground extinctions and luminosities for our objects, based on the spectral types given in Table 6. Allard & Hauschildt 1995b show that model spectra for solar metallicity M dwarfs change little within the range of surface gravities relevant for our objects. We have adopted the extinction law of Rieke & Lebofsky 1985; as discussed in Sect. 2.1, this law adequately reproduces the extinction vector traced by background sources in Chamaeleon I in the  $(J - H)$ ,  $(H - K)$  diagram. At visible wavelengths, departures from the universal extinction

law have been found in Chamaeleon I (Steenman & The 1989, Whittet et al. 1987). To minimize their effect, we have based the extinction estimates on the  $I$  and  $H$  bands, under the assumptions that  $I$  is at a long enough wavelength to be free from anomalous extinction effects, and that  $H$  is short enough not to be affected by circumstellar emission. At the  $J$  band, where the continuum spectral energy distributions of our newly found low mass sources peak, the extinction  $A_J$  is:

$$A_J = 0.919 [(I - H) - (I - H)_0] \quad (4)$$

where  $(I - H)$  and  $(I - H)_0$  are respectively the observed and intrinsic color indices. For the cases in which no  $H$  measurements are available, namely Sz23 and our new object Cha H $\alpha$ 6, a formula analogous to Eq. (4) has been used instead, replacing the  $(I - H)$  index by  $(V - I)$ , and the numerical coefficient by 0.544.

The luminosity  $L$  is:

$$\log L(L_\odot) = 1.86 - 0.4[J - A_J - DM + (V - J)_0 + BC] \quad (5)$$

where  $J$  is the measured  $J$  magnitude,  $DM = 5.73$  is the distance modulus (Sect. 3.2.2), and  $BC = M_{bol} - M_V$  is the bolometric correction. Again, for those cases for which only  $V$  and  $I$  are available, an equivalent form of Eq. (5) has been used, in which the term between square parentheses has been replaced by  $[V - 3.55A_J - DM + BC]$ .

Luhman & Rieke 1998 compare existing spectral type-temperature calibrations. Following their recommendation, we have adopted their best fit to the calibration of Leggett et al. 1996, which in turn is based on fits to synthetic spectra provided by cool model atmospheres. The temperature scale is in good agreement with that derived by Jones et al. 1996. Uncertainties in the temperature calibration of these models may be estimated to be around 200 K (Allard et al. 1997). Then, using the correspondences between spectral types and narrow band flux ratios of Prosser et al. 1991, we have transformed this calibration into:

$$T_{eff}(K) = 1922 + 818.6 (R_4/R_7) + 852.3 (R_3/R_2) \quad (6)$$

which includes the weighted average of the two flux ratios described above. Due to the flattening of the spectral type vs.  $(R_4/R_7)$  or  $(R_3/R_2)$  relationships at earlier spectral types, Eq. (6) is applicable only to spectral types M0 or later. A modified form of Eq. (6) has been used for Sz23, because  $(R_4/R_7)$  is not available in this case. For Cha H $\alpha$ 1, we have used directly the spectral subtype which enters the best-fit formula of Luhman & Rieke 1998.

Table 7 gives the resulting physical parameters, plus the extinction and the intrinsic infrared excess calculated as  $\Delta(H - K) = (H - K) - (H - K)_0 - 0.22A_J$ . Only the objects with spectral types M0 or later have been retained. The positions of the objects of Table 7 in the H-R diagram are plotted in Fig. 9, together with recent theoretical pre-main sequence evolutionary tracks. The comparison between different isochrones allows an estimate of the uncertainties in the physical parameters due to modeling alone, thus providing a lower limit to the uncertainties

**Table 7.** Physical parameters, extinctions and infrared excesses

Name	$T_{eff}$	$A_J$	$\log L(L_\odot)$	$\Delta(H - K)$
CHXR 73	3035:	2.0:	-0.79:	-0.23:
CHXR 74	3090	0.7	-0.82	0.04
B 34	3031	0.6	-1.18	0.07
HM 15	3712	1.6	0.12	0.55
Sz23	3448	0.7	-1.18	-
VW Cha	3794	1.1	0.51	0.49
CHXR78C	2940	0.6	-1.23	0.02
Cha H $\alpha$ 1	2600	0.4	-1.79	-0.06
Cha H $\alpha$ 2	2831	1.0	-1.16	-0.09
Cha H $\alpha$ 3	2824	0.6	-1.27	0.15
Cha H $\alpha$ 4	2781	0.2	-1.31	-0.01
Cha H $\alpha$ 5	2816	0.7	-1.06	0.07
Cha H $\alpha$ 6	2815	0.2	-1.57	-

**Table 8.** Ages and masses of low mass objects

Name	DAM97		B97	
	age (Myr)	mass ( $M_\odot$ )	age (Myr)	mass ( $M_\odot$ )
CHXR 73	0.5	0.14	1.5	0.15
CHXR 74	1	0.15	2	0.17
B 34	2	0.16	4	0.12
HM 15	0.3	0.3	-	-
Sz23	10	0.3	-	-
VW Cha	0.2	0.25	-	-
CHXR78C	2	0.14	3	0.09
Cha H $\alpha$ 1	0.3	0.03	0.5	0.03
Cha H $\alpha$ 2	1	0.10	0.4	0.08
Cha H $\alpha$ 3	1.5	0.09	0.5	0.075
Cha H $\alpha$ 4	1	0.08	0.5	0.065
Cha H $\alpha$ 5	0.5	0.10	0.4	0.09
Cha H $\alpha$ 6	3	0.08	2	0.06

Notes: DAM97 = D'Antona & Mazzitelli 1997 models, B97 = Burrows et al. 1997 models. The models of Burrows et al. 1997 reach up to  $0.237 M_\odot$ ; HM 15, Sz23, and VW Cha are out of their model grid.

in derived mass and ages. As expected, the results are somewhat model-dependent; nevertheless, they agree qualitatively that at least five of the new emission line objects are very young, with ages of  $3 \times 10^6$  years or less, and masses near the hydrogen-burning limit. From the preceding section, it appears that most of the stars in the infrared survey are of similar age; there is no significant older population with negligible H $\alpha$  emission. The young age for these objects may simply reflect the fact that Chamaeleon I is of too low a density to be gravitationally bound, so older stars will have wandered far from their formation sites. Of course, it may be possible as well that star formation in Chamaeleon I has simply taken place only in the last 3 Myr. The ages and luminosities of our objects as determined from both sets of isochrones are given in Table 8.

Although some of the new emission line objects may be brown dwarfs according to both sets of pre-main sequence evo-

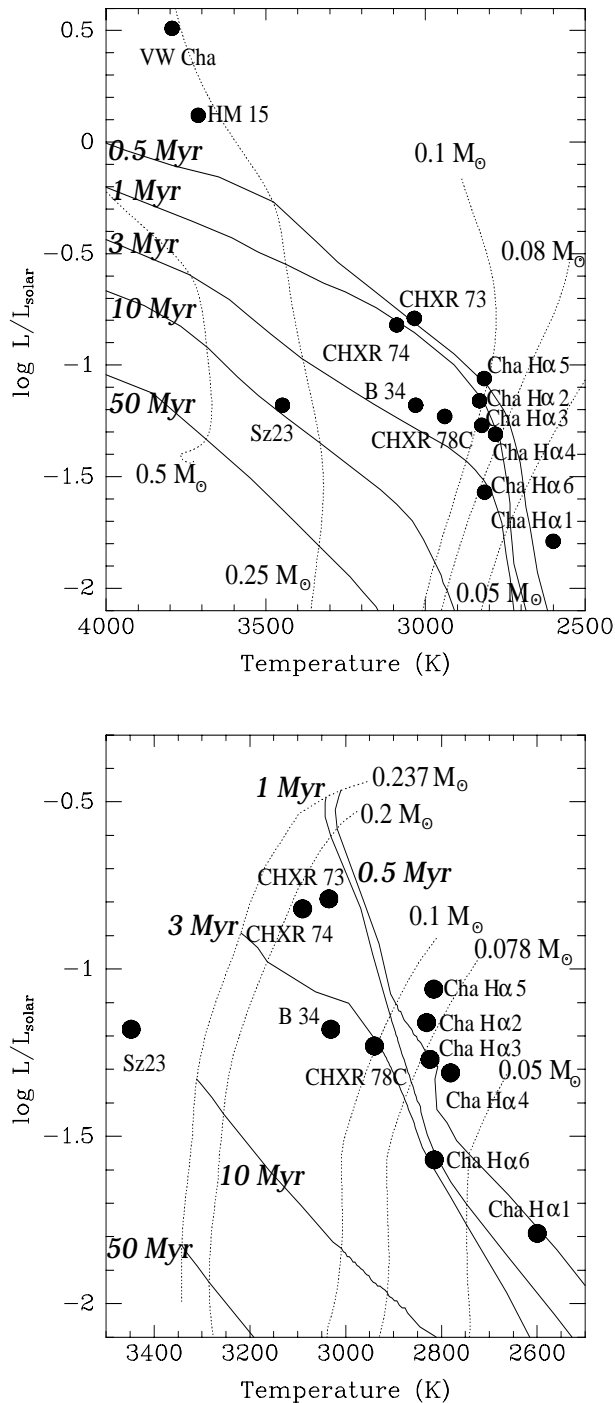


**Fig. 9.** H-R diagram with the position of our objects, superimposed on the pre-main sequence evolutionary tracks of D’Antona & Mazzitelli 1997 (*top panel*) and Burrows et al. 1997 (*bottom panel*). The solid lines represent equal ages, and the dotted lines equal masses. Note the difference in scales between both plots.

lutionary tracks, confirmation awaits a more precise determination of  $T_{eff}$  than presently available and higher accuracy in the models. The exception is Cha H $\alpha$ 1, for which uncertainties in the photometric measurements, the spectral classification, the temperature calibration, or the evolutionary tracks all seem to

be insufficient to move it into the region of hydrogen-burning main sequence stars. It can be therefore considered as a *bona-fide* brown dwarf (NC98).

### 3.4. Objects with near-infrared excess

Strom et al. 1989, 1993 have studied the incidence of K-band excesses in Taurus-Auriga. This work should be particularly relevant for comparison with Chamaeleon I because of the low density of young stars in both systems. It is expected that the incidence of disks, or their lifetimes, may be affected in very dense environments. These studies found 22 of 48 sources younger than 3 Myr to have detectable K excesses (greater than 0.2 magnitudes), while 10 of 23 sources between 3 and 10 Myr in age had such excesses. Given the age distribution for objects in the Chamaeleon I field, we would predict that about 40% of them would have excesses, based on this work. This prediction is consistent with other observations: 14 sources with IR excess out of 74 X-ray detections in the entire Chamaeleon I complex (LFH96), 7 out of 21 in L1495E in Taurus (Strom & Strom 1994), 19 out of 28 in  $\rho$  Ophiuchi (Casanova et al. 1995; the *JHK* photometry used is from the compilation of J. Carpenter, private communication by T. Greene), and 5 out of 19 in NGC 2024 (Freyberg & Schmitt 1995; Comerón et al. 1996). Taking all these data, the overall proportion of excess objects is 35%. Assuming an IMF slope of  $0.5 < \alpha < 1.0$ , an age of 3 Myr, and a 35 to 40% incidence of excesses, from Table 3b we would predict 4 to 8 objects in the infrared survey with infrared excesses. If  $\alpha$  were as large as 1.5, there should be  $\sim 16$  to 20 objects with excesses.

We identify excesses on the  $(J - H)$ ,  $(H - K)$  diagram (Lada & Adams 1992, Meyer et al. 1997). Circumstellar disks produce a  $(H - K)$  color redder than that corresponding to a stellar photosphere obscured by foreground dust for a given  $(J - H)$ . If the disk emission is intense enough in the *K* band, the position of an object in a  $(J - H)$ ,  $(H - K)$  diagram is shifted to the right of the reddening vector to a region inaccessible to normal reddened photospheres.

We find only three faint objects with probable excesses, in rough agreement with the predictions for  $0.5 < \alpha < 1.0$  but somewhat lower than expected. The detected excesses are far below the prediction for  $\alpha=1.5$ . The individual data for these objects are listed in Table 9. The third object in the list has its *J* and *H* magnitudes near the limits of acceptable precision of our survey. Consequently, its color indices, especially  $(J - H)$ , are rather uncertain, and its actual location to the right of the limiting reddening vector is doubtful. The mass, temperature, and extinction for three possible ages have been estimated following the procedure described in detail by Comerón et al. 1996a, 1998.

The unknown ages of these faint Chamaeleon I members makes it difficult to assess their true character. If we assume age estimates from those derived for the brighter members, they may all be brown dwarfs. However, the age distribution of the brighter members of Chamaeleon I is very sensitive to the adopted set of theoretical isochrones, as illustrated by LFH96

**Table 9.** Faint sources to the right of the limiting reddening vector

Name	R.A. (J2000.0)	dec (J2000.0)	$J$	$J - H$	$H - K$	age (Myr)	$M (M_{\odot})$	$T$ (K)	$A_V$
IR-1	11:06:42.7	-77:35:57	15.44	1.74	1.21	1	0.05	2850	11
						3	0.06	2850	11
						10	0.3	3500	13
IR-2	11:07:32.9	-77:37:53	17.67	2.29	1.46	1	0.03	2750	15
						3	0.04	2800	16
						10	0.12	3150	17
IR-3	11:08:41.2	-77:37:15	17.92	1.25	0.90	1	< 0.02	< 2650	< 5
						3	< 0.02	< 2600	< 5
						10	< 0.02	< 2600	< 5

(see also the discussion in Luhman & Rieke 1998 on the L1495E stellar population). It is therefore possible that the two brighter objects are of stellar mass, while the status of third object is uncertain because of possible photometric errors. Nonetheless, these objects illustrate the advantage of identifying cluster members through infrared excesses; it allows isolation of a portion of the very low luminosity cluster population.

The incidence of infrared excess among the brighter sources can be determined by comparison with the X-ray detections. It is likely that all nine previously known members of Chamaeleon I have been detected by ROSAT (see discussion in Sect. 3.2.2), but five of them have  $JHK$  colors compatible with having no near infrared excess. We could not find  $JHK$  photometry for HM 16, which appears saturated in our images. However, its strong  $H\alpha$  emission (Henize & Mendoza 1973) suggests that it should fall to the right of the reddening line, given that all the other bright objects of Table 2 for which strong  $H\alpha$  emission has been detected do appear in that region of the  $(J - H)$ ,  $(H - K)$  diagram. Therefore, four out of the nine would be selected as members on the basis of their infrared excess, in excellent agreement with the prediction that 35–40% of these objects would behave in this way.

Given the “normal” portion of excesses among the more luminous sources, the small number of objects with  $K < 14$  and detectable infrared excesses in the  $(J - H)$ ,  $(H - K)$  diagram may be a result in part of observational biases and small number statistics. To assess the expected detection rate better, we used available  $JHK$  photometry of faint members in other nearby stellar populations with intrinsic properties similar to those in Chamaeleon. First, we considered the faint objects of L1495E whose  $JHK$  photometry is given by Strom & Strom 1994. This region is similar to Chamaeleon I in that it contains a sparse population of lightly embedded young stellar objects, and moreover it lies at nearly the same distance from the Sun. We find in Tables 3 and 6 of Strom & Strom 1994 fourteen objects with  $J > 12$  and uncertainties in  $J$ ,  $H$ , and  $K$  of 0.1 mag or less. Their position in the  $(J - H)$ ,  $(H - K)$  diagram is plotted in Fig. 10 (open triangles); three of them lie to the right of the limiting reddening vector. We also plotted in Fig. 10 (open pentagons) the location of the six candidate brown dwarfs in the  $\rho$  Ophiuchi cloud core observed by ISO (Comerón et al.

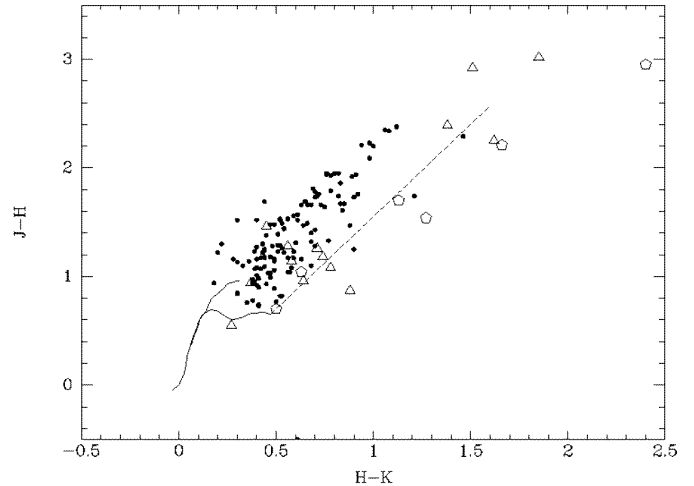


**Fig. 10.** Infrared color-color diagram displaying the position of the objects in the Chamaeleon I region and a limiting reddening vector as in Fig. 1, plus the faint L1495E sources (open triangles) and the brown dwarf candidates of  $\rho$  Ophiuchi (open pentagons).

1998), whose masses are relatively well constrained by fits to their spectral energy distributions. Four of them lie in the region characteristic of near infrared excesses produced by circumstellar disks. The combined results for L1495E and  $\rho$  Ophiuchi thus indicate that circumstellar excesses detectable through the position of the objects in the  $(J - H)$ ,  $(H - K)$  diagram are not substantially less common for very low mass stars and brown dwarfs than for more massive stars, despite the low temperatures of the former. This has been recently confirmed by Wilking et al. 1998, who have identified excess fluxes in the  $K$  band in a number of brown dwarfs in  $\rho$  Ophiuchi. The small number of low luminosity sources with excesses in Chamaeleon I therefore places an upper limit of  $\alpha < 1$  for the low mass IMF.

### 3.5. X-ray properties of the very low mass members

As already reported in NC98, the brown dwarf Cha  $H\alpha 1$  is clearly detected and identified with the X-ray source RXJ 110716–773552 (source XP 30 in Braun 1992), while Cha  $H\alpha 3$  and 6 are barely detected ( $4\sigma$ ). None of these three sources were detected earlier, neither in an Einstein Observa-

tory X-ray image due to much lower sensitivity, nor in an earlier analysis of the 5 ksec PSPC pointing. Cha H $\alpha$ 2 is very close to another, partly elongated, bright X-ray source, identified here as CHXR 26, unresolvable with the PSPC (cf. Fig. 3). Cha H $\alpha$ 5 is clearly undetected and upper limits are given in NC98.

The modest spectral resolution of the PSPC allows some spectral analysis. In particular, we can estimate so-called X-ray hardness ratios (X-ray colors) defined as follows: if  $Z_{s,m,h}$  are the count rates in the bands soft (0.1 to 0.4 keV), medium (0.5 to 0.9 keV), and hard (0.9 to 2.1 keV), respectively, then hardness ratios are given by

$$HR 1 = \frac{Z_h + Z_m - Z_s}{Z_h + Z_m + Z_s} \quad \text{and} \quad HR 2 = \frac{Z_h - Z_m}{Z_h + Z_m}$$

Hence, by definition, hardness ratios can range from  $-1$  to  $+1$ . If, for any particular source, no soft source were detected, then one can only give a lower limit to the hardness ratio  $HR 1$ , the upper limit being  $HR 1 = 1$ .

The hardness ratios measured for the Chamaeleon I members (Table 10) are consistent with  $\sim 1$  keV Raymond-Smith (Raymond & Smith 1977) spectra of solar abundance absorbed by the foreground column density as given in Table 7. To obtain X-ray fluxes, we divide the count rates by the appropriate energy conversion factor, namely  $10^{11}$  cts  $\text{cm}^2 \text{erg}^{-1}$  (see Neuhäuser et al. 1995 for details).

In Table 10, we compile the X-ray data of the Chamaeleon I members studied here. We list source designation, offset between optical and X-ray source position, maximum likelihood  $ML$  of source existence, effective exposure time, background and vignetting corrected counts in the broad band (0.1 to 2.4 keV), hardness ratios, X-ray luminosity  $L_X$  (at 160 pc) and the ratio of the X-ray to bolometric luminosity, with  $L_{bol}$  from either our Table 7 or LFH96.

In addition, we also calculate (and list in Table 10) the upper limits to X-ray emission of the low-mass (brown dwarf) candidates found with our IR survey (Table 9); the second object (IR-2), though, is located too close to LH $\alpha$  332-17 to be resolved with the PSPC, so that no upper limit can be given.

#### 4. Discussion

In view of the small-number statistics, and the assumptions involved in modeling, the results described in Sect. 3.2 do not firmly establish the slope of the low mass IMF in Chamaeleon I. However, from the estimates presented in Table 3, from the comparisons between observed and predicted numbers presented in Fig. 3, and from the low incidence of infrared excess sources, we conclude that the slope is rather shallow, in the range  $\alpha = 0.5$ – $1$  in linear mass units. This behavior is equivalent at low masses to an IMF rising slowly with increasing mass or being flat, if expressed in logarithmic mass units. Our result is consistent with recently determined mass functions of nearby open, emerged clusters such as the Pleiades (Festini 1997, and references therein), Praesepe (Williams et al. 1995), and the Hyades (Leggett et al. 1994). It also agrees with the results for younger aggregates such as  $\rho$  Ophiuchi (Comerón et al. 1993, Strom et

al. 1995), NGC 2024 (Comerón et al. 1996a), the Taurus clouds (Strom & Strom 1994), L1495E (Luhman & Rieke 1998) and IC 348 (Luhman et al. 1998). An exception to this behavior may be the Lupus clouds, where Hughes et al. 1994 find an excess of low mass stars over the predictions of the Miller & Scalo 1979 initial mass function. The greater distance to this complex resulting from a revision using *Hipparcos* data (Wichmann et al. 1998) may remove this apparent discrepancy, although the results of Knude & Høg 1998, also based on *Hipparcos*, cast some doubts on whether the distance is really higher, or actually lower, than the values adopted so far. The field initial mass function is more difficult to determine, due to factors such as the non-coevality, the uncertainties in the mass-luminosity transformation (Tinney 1993), or the observational effects of binarity at different distances (Kroupa 1995a, 1995b), but a shallow mass function also seems to reproduce the observations (Jarrett et al. 1994).

The very low mass population in the surveyed region seems to be younger than  $3 \times 10^6$  years. This is in overall agreement with the results of LFH96, who found that over 60% of the Chamaeleon I members in their list had ages of  $5 \times 10^6$  years or less when derived from the D’Antona & Mazzitelli 1998 tracks; however, for their five objects in common with our H $\alpha$  observations (CHXR 73, CHXR 74, CHXR 78C, VW Cha, and HM 15) we tend to find somewhat younger ages and lower masses. The differences are mostly due to the somewhat later spectral types that we derive and different temperature-spectral type calibration used, rather than to differences in the two sets of D’Antona & Mazzitelli tracks, which are not noticeable at the level of accuracy attainable with our observations.

Although we have detected few low luminosity sources with near infrared excesses in Chamaeleon I, we show that this result is probably largely due to small-number statistics. Taken together, the incidence of excesses for low luminosity members of low density clusters is similar to that for their higher luminosity members. One would expect a selection effect against detection of excesses in low mass objects. With cool spectral energy distributions, these objects will exhibit a relatively high H $\alpha$  equivalent width for a given amount of ionized gas, and their photospheric emission will be relatively bright at K, tending to dominate any excess. Thus, one predicts a decreasing incidence of excesses as a function of H $\alpha$  equivalent width, as well as in general. The detection of excesses in significant numbers over the full sample of low luminosity members of nearby, low density clusters therefore is an interesting conclusion.

Models of near infrared emission of circumstellar disks (Lada & Adams 1992, Calvet et al. 1991, 1992, Meyer et al. 1997) successfully reproduce the observational *locus* of T Tauri stars in the  $(J - H)$ ,  $(H - K)$  diagram, but do not extend to the temperatures and luminosities of the faintest sources in our study. However, some features in models for higher mass objects suggest that circumstellar disks around brown dwarfs should not be conspicuous in the  $(J - H)$ ,  $(H - K)$  diagram. For their fiducial central star of  $\mathcal{M} = 0.5 M_\odot$ ,  $R = 1.8 R_\odot$ , and  $T = 4000$  K, Meyer et al. 1997 found that accretion rates below  $10^{-8} M_\odot \text{yr}^{-1}$  do not contribute to the disk luminosity

**Table 10.** X-ray data for Chamaeleon I cloud members studied here

Designation	pos. offset	detection level ( $ML$ )	exp. [ksec]	X-ray counts (broad band)	hardness ratios		$\log L_X$ [erg/s]	$\log L_X/L_{bol}$
					HR 1	HR 2		
CHXR 73	15.9''	91	37.8	61.9 ± 10.0	0.48 ± 0.21	0.67 ± 0.13	28.70 ± 0.06	-4.10
CHXR 74	1.9''	257	36.7	118.9 ± 12.3	≥ 0.86	0.37 ± 0.09	28.99 ± 0.05	-3.78
B 34	5.2''	130	37.8	73.3 ± 10.1	≥ 0.69	0.31 ± 0.13	28.77 ± 0.05	-3.64
HM 15	7.3''	460	37.1	178.1 ± 15.1	0.96 ± 0.06	0.68 ± 0.06	29.16 ± 0.04	-4.55
Sz 23, VW Cha	(1)	6856	35.9	1576.5 ± 40.7	0.98 ± 0.01	0.43 ± 0.02	30.12 ± 0.02	(1)
HM 16, HD 97048	(2)	161	37.1	89.7 ± 11.7	0.76 ± 0.13	0.74 ± 0.09	28.87 ± 0.05	(2)
Glass I (3)	5.3''	4086	37.5	947.4 ± 31.5	0.95 ± 0.02	0.37 ± 0.03	29.88 ± 0.02	-4.75
CHXR 78 C	3.5''	61	37.6	59.4 ± 10.0	0.57 ± 0.22	0.12 ± 0.17	28.68 ± 0.07	-3.68
LH $\alpha$ 332-17	7.1''	5634	37.4	1221.7 ± 35.7	≥ 0.98	0.49 ± 0.03	30.00 ± 0.01	-4.65
CHXR 26	4.7''	519	37.8	194.9 ± 15.2	0.85 ± 0.07	0.66 ± 0.06	29.19 ± 0.04	-4.34
Cha H $\alpha$ 1	4''	33.7	37.8	31.4 ± 7.7	≥ 0.40	0.15 ± 0.22	28.40 ± 0.10	-3.44
Cha H $\alpha$ 2	not resolved, 29'' SE of X-ray source identified as CHXR 26							
Cha H $\alpha$ 3	16.8''	11.8	37.6	11.9 ± 5.7	≥ 0.13	0.04 ± 0.35	27.98 ± 0.17	-4.31
Cha H $\alpha$ 4	not detected		34.8	≤ 22.9			≤ 28.30	≤ -4.91
Cha H $\alpha$ 5	not detected		33.9	≤ 1.98			≤ 27.25	≤ -5.24
Cha H $\alpha$ 6	10''	8.1	31.8	8.2 ± 3.4	≥ 0.26	0.08 ± 0.40	27.89 ± 0.15	-4.09
IR-1 (3)	not detected		30.7	≤ 4.7			≤ 27.67	≤ -4.49
IR-2	not resolved, located too close to bright X-ray source LH $\alpha$ 332-17							
IR-3	not detected		34.0	≤ 5.3			≤ 27.67	

*Remarks:* (1) X-ray source confusion: Both VW Cha and Sz 23 are very close (3.0 and 11.4 arc sec, respectively) to this X-ray source, which is too close to be resolved spatially with the ROSAT PSPC.

(2) X-ray source confusion: HM 16 and HD 97048 are very close to this elongated, spatially unresolved X-ray source.

(3) We use  $L_{bol} = 8.5 \cdot L_{\odot}$  for Glass I, and  $L_{bol} = 0.029 \cdot L_{\odot}$  for IR-1, both from our photometry.

via viscous heating. The accretion rates to be expected for massive brown dwarfs are of this order, unless we are witnessing a transient stage of rapid accretion; otherwise, steady accretion in excess of  $10^{-8} M_{\odot} \text{ yr}^{-1}$  sustained over  $\sim 10^7$  yr would end up by giving a low mass star, rather than a brown dwarf. Moreover, the rate of viscous heating depends on the potential well created by the central object, which is much smaller for a brown dwarf than for a  $M = 0.5 M_{\odot}$  star: the radii of both objects are comparable, whereas the mass differs by one order of magnitude. Therefore, only irradiation by the central object is left as a source of luminosity for the circumstellar disk. This may be insufficient to produce a significant flux excess at  $K$  if the disk has a central hole, a feature inferred by Meyer et al. 1997 to be common among young stellar objects. Thus, further observational and theoretical study of the behavior of disks around very low mass young objects would be of great interest.

Concerning the high energy emission properties of the M-type stars studied here (Table 10), we find X-ray to bolometric luminosity ratios ranging from -4.75 to -3.64, which is quite typical for X-ray active M-type stars. In this regard, the Herbig Ae/Be star LH $\alpha$  332-17 appears to be quite typical for X-ray emission of Herbig Ae/Be stars (cf. Zinnecker & Preibisch 1994). The detection of an X-ray emitting brown dwarf in Chamaeleon I shows that the luminosity ratios quoted above extend beyond the end of the main sequence. It is doubtful however to what extent this applies to young brown dwarfs only, as an extensive search for X-ray emission from known brown dwarfs

has failed to provide any detections among more evolved objects (Neuhäuser et al. 1999).

## 5. Conclusions

We have presented the results of a deep objective prism survey in the H $\alpha$  region and a near-infrared imaging survey, aimed at the study of the initial mass function for very low mass stars and brown dwarfs in the densest region ( $10' \times 10'5$ ) of the Chamaeleon I star forming cloud. We have also analyzed very deep pointed X-ray observations which include the area surveyed in H $\alpha$  and the infrared. We introduce a new approach to separate the cloud members from the background, a critical issue in studying this sparse cluster. We find that:

1. The initial mass function below  $M \sim 0.2 M_{\odot}$  can be constrained to have a rather shallow slope. When the initial mass function  $\Phi(\mathcal{M})$  is approximated by a power law of the form  $\Phi(\mathcal{M})d\mathcal{M} \propto M^{-\alpha}d\mathcal{M}$ , the index  $\alpha \simeq 0.5-1.0$ . This behavior is equivalent to an IMF that is flat or slowly rising to  $0.2 M_{\odot}$  in logarithmic mass units.
2. The low mass IMF in Chamaeleon I is therefore similar to that observed in most other young clusters, regardless of their density.
3. Six new objects are found in our H $\alpha$  survey. A comparison to recent theoretical pre-main sequence tracks shows that they are very young (ages near or below  $3 \times 10^6$  years) with masses near the hydrogen burning limit, and even below in at least one case.

4. In addition, two, or possibly three, fainter objects are detected by means of their position in the  $(J - H)$ ,  $(H - K)$  diagram, indicative of the existence of circumstellar material. They have luminosities and colors consistent with being brown dwarfs if their ages are below  $10^7$  yr.

5. The relatively high incidence of circumstellar excesses around very low luminosity objects may be in conflict with simple extrapolation of theoretical models of higher luminosity objects. To explore this behavior, modeling is needed for accretion rates around  $10^{-8} M_{\odot} \text{ yr}^{-1}$  irradiated by a low luminosity central object with a temperature under 3000 K.

6. X-ray emission properties of the young late type stars in the surveyed area are similar to those of the overall population of X-ray active M-type stars. Moreover, the detection of a X-ray emitting brown dwarf with a derived mass of only  $0.05 M_{\odot}$  incorporates brown dwarfs as a new class of X-ray emitters, with a X-ray to bolometric luminosity ratio similar to that of late M-type stars.

*Acknowledgements.* It is a pleasure to thank the 2p2 Team at ESO-La Silla for their assistance during the observations, particularly the support astronomer, Dr. Jesper Storm, and the telescope operators, Sres. Luis Ramírez and Rolando Vega. The ESO Director's Discretionary Time Committee is acknowledged for its allocation of time to this project. The valuable introduction of Dr. James Brewer to the use of DFOSC and the 1.5 Danish telescope did much to improve the efficiency of the spectroscopic observations. Dr. Giovanni Carraro is thanked for having allowed us to use some non-photometric minutes of his time at the NTT to obtain the spectrum of Cha H $\alpha$ 1 presented here. Dr. Chris Lidman kindly allowed us to include that same object in the list of targets to be observed in the commissioning of SOFI. Drs. Adam Burrows and Francesca D'Antona kindly provided us with results of their recent models in machine-readable form. We also thank Dr. Eric Feigelson, the PI of the shorter X-ray observation, for allowing us to use his 2nd processing data. Drs. Göran Olofsson and Anlaug Amanda Kaas are thanked for having provided near infrared and ISO data prior to publication, Dr. Warrick A. Lawson for having kindly made available published data in machine-readable form, and Dr. Tom Greene for making available to us the compilation of  $\rho$  Ophiuchi photometry of John Carpenter, and Dr. Kevin Luhman for providing the comparison spectra shown in Fig. 8. Comments from the referee, Dr. Jens Knude, helped us to significantly improve the contents of this paper. This work was supported by the NATO Collaborative Research Grant CRG 940671 and NASA grant NAGW-4083. RN wishes to thank the Deutsche Forschungs Gemeinschaft for financial support in their Star Formation program. ROSAT is supported by the Max-Planck-Society and the German Government (BMBF/DLR).

## References

- Alcalá J.M., Krautter J., Schmitt J.H.M.M., et al., 1995, A&AS, 114, 109
- Alcalá J.M., Covino E., Neuhauser R., Schmitt J.H.M.M., Wichmann R., 1997, A&A 319, 184
- Allard F., Hauschildt P.H., 1995a, ApJ 445, 433
- Allard F., Hauschildt P.H., 1995b, In: Tinney C. (ed.) The bottom of the main sequence -and beyond. Springer-Verlag
- Allard F., Hauschildt P.H., Alexander D.R., Starrfield S., 1997, ARA&A 35, 137
- Baud B., Young E., Beichman C.A., et al., 1984, ApJ 278, L53
- Bessell M.S., Brett J.M., 1988, PASP 100, 1134
- Braun M., 1992, Diploma Thesis, Friedrich-Schiller Universität Jena
- Burrows A., Hubbard W.B., Saumon D., Lunine J.I., 1993, ApJ 406, 158
- Burrows A., Marley M., Hubbard W.B., et al., 1997, ApJ 491, 856
- Calvet N., Patiño A., Magris G., D'Alessio P., 1991, ApJ 380, 617
- Calvet N., Magris G., Patiño A., D'Alessio P., 1992, RMxAA 24, 27
- Cambrésy L., Epchtein N., Copet E., et al., A&A 324, L5
- Cambrésy L., Copet E., Epchtein N., et al., 1998, A&A 338, 977
- Carter B.S., Meadows V.S., 1995, MNRAS 276, 734
- Casanova S., Montmerle T., Feigelson E.D., André P., 1995, ApJ 439, 752
- Comerón F., Rieke G.H., Burrows A., Rieke M.J., 1993, ApJ 416, 185
- Comerón F., Rieke G.H., Rieke M.J., 1996a, ApJ 473, 294
- Comerón F., Torra J., Rieke G.H., 1996b, A&A 308, 565
- Comerón F., Rieke G.H., Claes P., Torra J., Laureijs R.J., 1998, A&A 335, 522
- Covino E., Alcalá J.M., Allain S., et al., 1997, A&A 328, 187
- D'Antona F., Mazzitelli I., 1994, ApJS 90, 467
- D'Antona F., Mazzitelli I., 1997, Mem. S. A. It. 68, 807
- Feigelson E.D., Casanova S., Montmerle T., Guibert J., 1993, ApJ 416, 623
- Festin L., 1997, A&A 322, 455
- Freyberg M.J., Schmitt J.H.M.M., 1995, A&A 296, L1
- Gauvin L.S., Strom K.M., 1992, ApJ 385, 217 (GS92)
- Hartigan P., 1993, AJ 105, 1511
- Henize K.G., Mendoza E.E., 1973, ApJ 180, 115
- Herbig G.H., 1998, ApJ 497, 736
- Huenemoerder D.P., Lawson W.A., Feigelson E.D., 1994, MNRAS 271, 967
- Hughes J., Hartigan P., Krautter J., Kelemen J., 1994, AJ 108, 1071
- Hyland A.R., Jones T.J., Mitchell R.M., 1982, MNRAS 201, 1095
- Kenyon S.J., Hartmann L., 1995, ApJS 101, 117
- Kirkpatrick J.D., Henry T.J., McCarthy D.W., 1991, ApJS 77, 417
- Kirkpatrick J.D., Kelly D.M., Rieke G.H., et al., 1993, ApJ 402, 643
- Kirkpatrick J.D., Henry T.J., Simons D.A., 1995, AJ 109, 797
- Knude J., Høg E., 1998, A&A 338, 897
- Kroupa P., 1995a, ApJ 453, 350
- Kroupa P., 1995b, ApJ 453, 358
- Jarrett T.H., Dickman R.L., Herbst W., 1994, ApJ 424, 852
- Jones H.R.A., Longmore A.J., Jameson R.F., Mountain C.M., 1994, MNRAS 267, 413
- Jones H.R.A., Longmore A.J., Allard F., Hauschildt P.H., 1996, MNRAS 280, 77
- Lada C.J., Adams F.C., 1992, ApJ 393, 278
- Lawson W.A., Feigelson E.D., Huenemoerder D.P., 1996, MNRAS 280, 1071 (LFH96)
- Leggett S.K., Allard F., Berriman G., Dahn C.C., Hauschildt P.H., 1996, ApJS 104, 117
- Leggett S.K., Harris H.C., Dahn C.C., 1994, AJ 108, 944
- Luhman K.L., Rieke G.H., 1998, ApJ 497, 354
- Luhman K.L., Liebert J., Rieke G.H., 1997, ApJ 489, L165
- Luhman K.L., Rieke G.H., Lada C., Lada E., 1998, ApJ 508, 347
- Martín E.L., Zapatero-Osorio M.R., Rebolo R., 1996, ApJ 469, 706
- Miller G.E., Scalo J.M., 1979, ApJS 41, 513
- Meyer M.R., Calvet N., Hillenbrand L.A., 1997, AJ 114, 288
- Neuhauser R., Comerón F., 1998, Sci 282, 83
- Neuhauser R., Sterzik M.F., Schmitt J.H.M.M., Wichmann R., Krautter J., 1995, A&A 297, 391
- Neuhauser R., Briceño, C., Comerón F., et al., 1999, A&A 343, 151

- Nordh L., et al., 1996, *A&A* 315, L185
- Olofsson G., et al., 1998, In: *Brown dwarfs and extrasolar planets*. ASP Conf. Ser. 134
- Pfeffermann E., et al., 1988, The focal plane instrumentation of the ROSAT telescope. In: *Proc. SPIE* 733, 519
- Prosser C.F., Stauffer J., Kraft R.P., 1991, *AJ* 101, 1361
- Raymond J.C., Smith B.S., 1977, *ApJS* 35, 419
- Reipurth B., Nyman L.-Å., Chini R., 1996, *A&A* 314, 258
- Rieke G.H., Lebofsky M.J., 1985, *ApJ* 288, 618
- Schwartz R.D., 1991, In: Reipurth B. (ed.) *Low Mass Star Formation in Southern Molecular Clouds*. ESO Sci. Rep. 11
- Steenman H., The P.S., 1989, *Ap&SS* 161, 99
- Strom K.M., Strom S.E., Edwards S., Cabrit S., Skrutski M.F., 1989, *AJ* 97, 1451
- Strom S.E., Edwards S., Skrutski M.F., 1993, In: Levy E.H., Lunine J.I., Mathews M.S. (eds.) *Protostars and Planets III*. University of Arizona Press, Tucson, 837
- Strom K.M., Strom S.E., 1994, *ApJ* 424, 237
- Strom K.M., Kepner J., Strom S.E., 1995, *ApJ* 438, 813
- Tinney C.G., 1993, *ApJ* 414, 279
- Trümper J.E., 1983, *Adv. Space Res.* 2, 241
- Wainscoat R.J., Cohen M., Volk K., Walker H.J., Schwartz D.E., 1992, *ApJS* 83, 111
- Whittet D.C.B., Kिरrane T.M., Kilkenny D., et al., 1987, *MNRAS* 224, 497
- Wichmann R., et al., 1998, *MNRAS* 301, L39
- Wilking B.A., McCaughrean M.J., Burton M.G., et al., 1997, *AJ* 114, 2029
- Wilking B.A., Greene T.P., Meyer M.R., 1998, *AJ* in press
- Williams S.D., Stauffer J.R., Prosser C.F., Herter T., 1994, *PASP* 106, 817
- Williams D.M., Rieke G.H., Stauffer J.R., 1995, *ApJ* 445, 359
- Zimmermann H.U., Becker W., Belloni T., et al., 1994, *EXSAS Users's Guide*. MPE Report 244, ROSAT Scientific Data Center, Garching
- Zinnecker H., Preibisch Th., 1994, *A&A* 292, 152